The DEAD box RNA helicase DDX42 is an intrinsic inhibitor of positive-strand RNA viruses

Boris Bonaventure[1], Antoine Rebendenne[1#], Francisco Garcia de Gracia[1#], Joe McKellar[1#], Ségolène Gracias[2], Emmanuel Labaronne[3], Marine Tauziet[1], Ana Luiza Chaves Valadão[1], Eric Bernard[1], Laurence Briant[1], Nathalie Gros[4], Wassila Djilli[1], Mary Arnaud-Arnould[1], Valérie Courgnaud[5], Hugues Parrinello[6], Stéphanie Rialle[6], Emiliano Ricci[3], Nolwenn Jouvenet[2], Reiner Schulz[7], Olivier Moncorgé[1] and Caroline Goujon[1*]

1 IRIM, CNRS, Université de Montpellier, France

2 Institut Pasteur, Virus Sensing and Signaling Unit, Department of Virology, CNRS UMR 3569, Paris, France

3 LBMC, Université de Lyon, ENS de Lyon, CNRS, INSERM, Lyon, France

4 CEMIPAI, CNRS, Université de Montpellier, France

5 IGMM, CNRS, Université de Montpellier, France

6 Montpellier GenomiX (MGX), Biocampus, CNRS, INSERM, Université de Montpellier, France

7 Department of Medical & Molecular Genetics, King's College London, United Kingdom

[#] Contributed equally to the work

[*] Corresponding and lead author: Caroline Goujon, IRIM UMR9004, 1919 route de Mende, 34293 Montpellier cedex 5. Phone: +33 4 34 35 94 33, e-mail: caroline.goujon@irim.cnrs.fr, ORCID iD: 0000-0001-8571-1108

Abstract

Genome-wide screens are powerful approaches to unravel new regulators of viral infections. Here, we used a CRISPR/Cas9 screen to reveal new HIV-1 inhibitors. This approach led us to identify the RNA helicase DDX42 as an intrinsic antiviral inhibitor. DDX42 was previously described as a non-processive helicase, able to bind RNA secondary structures such as G-quadruplexes, with no clearly defined function ascribed. Our data show that depletion of endogenous DDX42 significantly increased HIV-1 DNA accumulation and infection in cell lines and primary cells. DDX42 overexpression inhibited HIV-1, whereas a dominant-negative mutant increased infection. Importantly, DDX42 also restricted retrotransposition of LINE-1, infection with other retroviruses and positive-strand RNA viruses, including CHIKV and SARS-CoV-2. However, DDX42 did not inhibit infection with three negative-strand RNA viruses, arguing against a general, unspecific effect on target cells, which was confirmed by RNA-seq analysis. DDX42 was found in the vicinity of viral elements by proximity ligation assays, and cross-linking RNA immunoprecipitation confirmed a specific interaction of DDX42 with RNAs from sensitive viruses. This strongly suggested a direct mode of action of DDX42 on viral ribonucleoprotein complexes. Taken together, our results show for the first time a new and important role of DDX42 in intrinsic antiviral immunity.

Introduction

The intrinsic and innate immunity are at the frontline against viral invasion and provide a rapid and global defence. The innate immunity relies on viral sensing by Pathogen Recognition Receptors (PRRs) inducing the production of type 1 and 3 interferons (IFNs). Secreted IFNs bind to specific receptors and activate the JAK-STAT signalling cascade, which leads to the expression of hundreds of IFN-stimulated genes (ISGs). The cellular reprogramming induced by ISG expression allows the establishment of an antiviral state that efficiently limits viral replication. Some ISGs are indeed direct antiviral effectors harbouring powerful antiviral activities (1). In addition to the IFN response, antiviral proteins that are constitutively expressed are able to immediately counteract incoming virus replication and are referred to as intrinsic inhibitors; they are part of the so-called intrinsic immunity.

Intensive efforts have been made over the past decades to identify genes able to limit viral replication. Several ISGs were identified a long time ago as major players of innate immunity against viruses, such as the myxovirus resistance protein 1 (MX1) Dynamin Like GTPase, 2′,5′-oligoadenylate synthetases (OASs) and ribonuclease L (RNASeL), or protein kinase R (PKR) (2–4). More recently, gain-of-function and loss-of-function screens have identified new IFN-induced antiviral effectors (5–7). A growing list of cellular proteins with various functions has hence been identified as capable of limiting different steps of virus life cycles (8–10). Viruses have often evolved to counteract the action of these so-called restriction factors. However, type 1 IFNs (e.g. IFN-alpha and -beta) induce, through the expression of ISGs, an antiviral state particularly efficient at inhibiting HIV-1 when cells are pre-exposed to IFN (9). The dynamin-like GTPase MX2, and, recently, the restriction factor TRIM5α, have both been shown to participate in the IFN-induced inhibition of HIV-1 (6, 11–13). While numerous antiviral ISGs have been identified, less is probably known about the extent of the intrinsic, antiviral inhibitor repertoire. The recent identification of TRIM7 as an intrinsic inhibitor of enteroviruses illustrates the fact that important antiviral inhibitors most certainly remain to be revealed (14).

72 With the hypothesis that additional HIV-1 inhibitors remained to be identified, we took advantage
73 of the hostile environment induced by IFN to develop a whole-genome, CRISPR/Cas9 screen
74 strategy in order to reveal intrinsic and innate inhibitors. This strategy led us to identify DDX42
75 as a new intrinsic inhibitor of HIV-1, acting independently of the IFN system. We reveal that
76 endogenous DDX42 is antiviral in various cell types, including primary targets of HIV-1, and
77 impairs the accumulation of viral DNA. Moreover, our data show a broad activity against
78 lentiviruses and the retrovirus Murine Leukemia Virus (MLV). Reminiscent of other HIV-1
79 inhibitors such as APOBEC3G, DDX42 also blocks LINE-1 spread by interacting with their
80 RNAs. Interestingly, while three different negative strand RNA viruses were found insensitive to
81 DDX42, several positive strand RNA viruses, including the flavivirus Zika (ZIKV), the alphavirus
82 Chikungunya (CHIKV) and the severe acute respiratory syndrome coronavirus 2 (SARS-CoV-2),
83 were inhibited by this non-processive RNA helicase. Finally, cross-linking RNA
84 immunoprecipitation assays showed that DDX42 specifically binds to viral RNAs from sensitive
85 viruses, strongly suggesting a direct mode of action. Overall, our study sheds light on a new
86 intrinsic, antiviral function of a so far poorly studied DEAD-box RNA helicase, and provide new
87 insights on a broad-spectrum antiviral inhibitor.
88
89 **Results**
90 The Genome-Scale CRISPR Knock-Out (GeCKO) sgRNA library (15–17) was used to generate
91 knock-out (KO) populations in the glioblastoma T98G cell line. This cell line is both highly
92 permissive to HIV-1 infection and potently able to suppress infection following type 1 IFN
93 treatment (Fig. S1A). The screen strategy is depicted in Figure 1A. Cas9-expressing T98G cells
94 were independently transduced with lentiviral vectors (LVs) coding the two-halves of the
95 GeCKO library, at a low multiplicity of infection (MOI). Next-generation sequencing showed
96 more than 94% sgRNA coverage for each sub-library (not shown). Cells were pre-treated with
97 type 1 IFN (IFN-alpha) and incubated with VSV-G-pseudotyped, HIV-1 based LVs coding for an
98 antibiotic resistance cassette. The cells which were successfully infected despite the IFN
99 treatment were selected by survival in the presence of antibiotics. In order to enrich the

100 populations with mutants of interest and to limit the presence of false-positives, two additional
101 rounds of IFN treatment, infection and selection (with different antibiotics) were performed. As
102 expected, the cells enriched after each round became less refractory to HIV-1 infection following
103 IFN treatment (Fig. S1B).

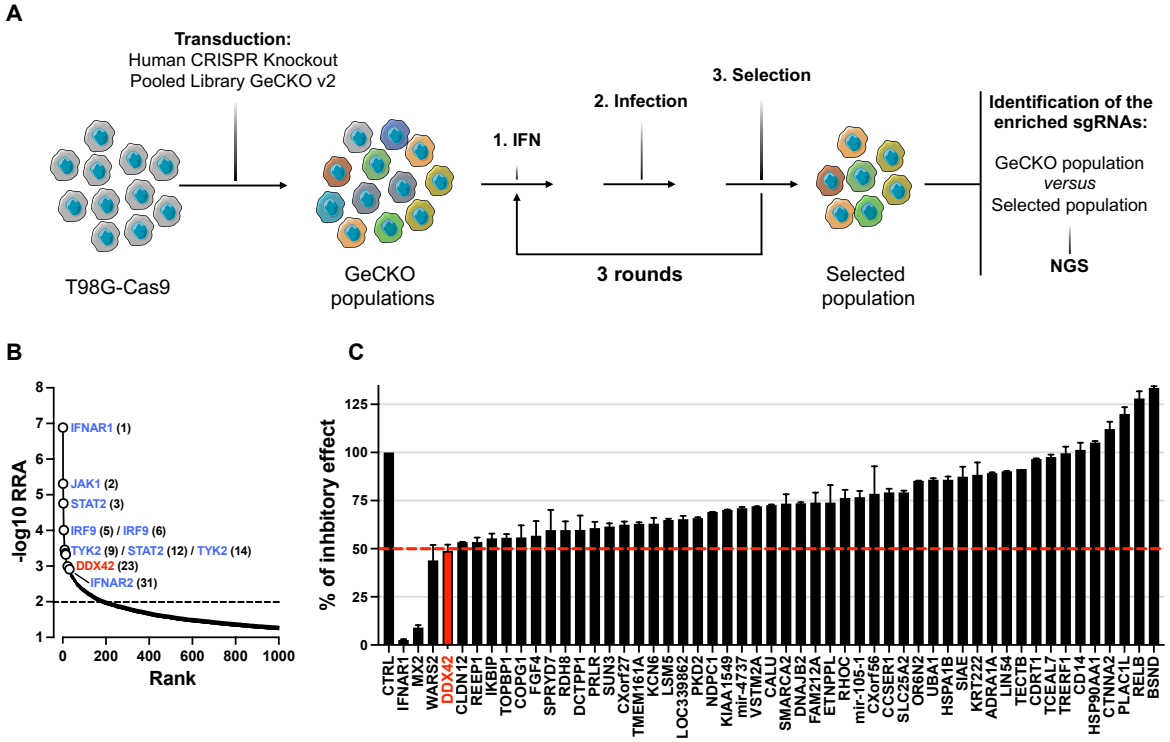

104

105 **Figure 1. A whole-genome CRISPR/Cas9 screen to identify new HIV-1 inhibitors.**
106 **A.** Screen strategy. GeCKO cell populations (obtained by transduction of T98G/Cas9 cells with GeCKO v2 LV
107 library) were IFN-treated, challenged with HIV-1 LVs coding for an antibiotic resistance gene and selected.
108 Three rounds of IFN treatment, infection and selection were performed. Genomic DNAs of initial GeCKO and 3-
109 time selected populations were extracted, the sgRNA-coding sequences amplified and sequenced.
110 **B.** Candidate gene identification. MAGeCK computational statistical tool (18) was used to establish a Robust
111 Rank Aggregation (RRA) score for each gene based on sgRNA enrichment and number of sgRNAs per gene.
112 Genes belonging to the type 1 IFN response pathway (in blue) and DDX42 (in red) are shown (respective ranks
113 into brackets) for 2 independent screens (the results of which were merged in the analysis).
114 **C.** Candidate validation. T98G/Cas9/CD4/CXCR4/Firefly KO populations were generated for the 25 top hits of
115 each screen. The control (CTRL) condition represents the mean of 4 negative CTRL populations, obtained with
116 4 non-targeting sgRNAs; *IFNAR1* and *MX2* KO populations were used as positive controls. KO cell populations
117 were treated with IFN and infected with HIV-1 Renilla and luciferase signals were measured 30 h later (Renilla
118 signals were normalized to Firefly). IFN inhibition (i.e. ratio of untreated / IFN-treated conditions) was calculated
119 and set at 100% inhibition for CTRL. A representative experiment is shown (mean and standard deviation from
120 technical duplicates).
121

122 The differential sgRNA abundance between the initial GeCKO populations and selected
123 populations was analysed by next-generation sequencing (NGS) and the MAGeCK algorithm
124 was used to rank the candidate genes (Fig. 1B). An enrichment was observed for 200 genes
125 (RRA score > 0,01), with the best hits being *IFNAR1*, *JAK1* and *STAT2* (Fig. 1B). The crucial
126 mediators of type 1 IFN signalling cascade were among the top hits in both screens (with the
127 notable exception of *STAT1*), validating our approach and confirming the identification of
128 relevant genes. Interestingly, most of the other candidates displayed unknown functions, or
129 functions that were *a priori* unrelated to innate immunity. Of note, very little overlap was
130 observed between the two independent screens, performed with two sub-libraries. However,
131 such a poor overlap between biological replicates has been observed before and does not
132 preclude obtaining valid data (19). The top 25 candidate genes from each screen were selected
133 for further validation. T98G/Cas9 cells expressing HIV-1 CD4 and CXCR4 receptors, as well as
134 Firefly luciferase as an internal control (T98G/Cas9/CD4/CXCR4/Firefly cells), were transduced
135 with sgRNA-expressing LVs to generate individual KO populations, using the identified sgRNA
136 sequences. Four irrelevant, non-targeting sgRNAs, as well as sgRNAs targeting *IFNAR1* and
137 *MX2*, were used to generate negative and positive control populations, respectively. The KO cell
138 populations were pre-treated with IFN and infected with an HIV-1 reporter virus expressing
139 Renilla luciferase and bearing HIV-1 envelope (20) (hereafter called HIV-1 Renilla). Infection
140 efficiency was analysed 30 h later (Fig. 1C). As expected (11, 21, 22), *IFNAR1* and *MX2* KO
141 fully and partially rescued HIV-1 infection from the protective effect of IFN, respectively. The KO
142 of two candidate genes, namely *WARS2* and *DDX42*, allowed a partial rescue of HIV-1 infection
143 from the IFN-induced inhibition, suggesting a potential role of these candidate genes in HIV-1
144 inhibition.
145
146 DDX42 is a member of the DEAD box family of RNA helicases, with RNA chaperone activities
147 (23) and, as such, retained our attention. Indeed, DEAD box helicases are well-known to
148 regulate HIV-1 life cycle (24). However, to our knowledge, the impact of DDX42 on HIV-1
149 replication had never been studied. In order to validate the effect of *DDX42* KO on HIV-1

150 infection in another model cell line, two additional sgRNAs were designed (sgRNA-2 and -3) and
151 used in parallel to the one identified in the GeCKO screen (sgDDX42-1) (Fig. 2A). U87-
152 MG/CD4/CXCR4 cells were used here, as we previously extensively characterized the IFN
153 phenotype in these cells (11). Control and *DDX42* KO cell populations were generated and pre-
154 treated or not with IFN prior to infection with HIV-1 Renilla. Of note, CRISPR/Cas9 KO of
155 *DDX42* induced only a partial decrease of DDX42 protein levels (Fig. 2A) and cell populations
156 tended to derive (not shown), suggesting a potential role for DDX42 in cell proliferation or long-
157 term survival. We observed however that DDX42 partial depletion with all 3 sgRNAs improved
158 HIV-1 infection, confirming that endogenous DDX42 had a negative impact on HIV-1 replication.
159 Interestingly, the increase in infection efficiency induced by *DDX42* KO was observed
160 independently of the IFN treatment. DDX42 is not an ISG, as shown in several cell lines (e.g.
161 U87-MG, T98G, HEK293T) and in primary T cells and monocyte-derived macrophages (Fig.
162 S2A and GSE46599 (11)). The fact that the IFN-induced state is at least partially saturable (Fig.
163 S1A) explains why an intrinsic inhibitor of HIV-1, which is not regulated by IFN, could be
164 identified by our approach. Indeed, removing one barrier to infection presumably rendered the
165 cells more permissive and, in this context, IFN had less of an impact on viral replication.

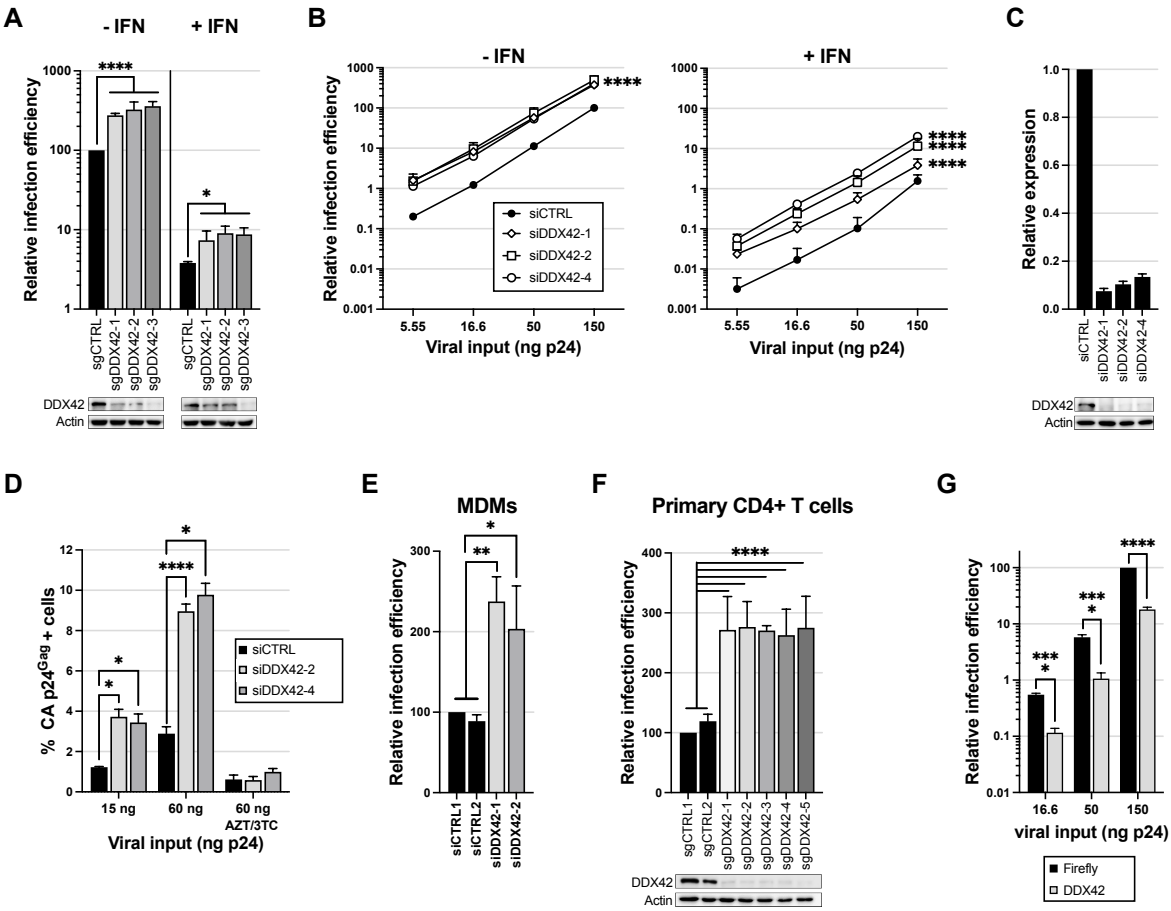

Figure 2. DDX42 is an intrinsic inhibitor of HIV-1.

A. Top: *DDX42* KO and CTRL KO U87-MG/CD4/CXCR4/Cas9/Firefly cells were generated using 3 sgRNAs and 4 non-targeting sgRNAs, respectively (for CTRL, the average of data obtained with 4 cell populations is shown). Cells were treated or not with IFN 24 h prior to infection with HIV-1 Renilla. Relative luminescence results for IFN-treated and -untreated conditions are shown. Two-way ANOVA on log-transformed data with Sidak's test. Bottom: Immunoblot analysis of DDX42 levels is shown for 1 CTRL and DDX42-depleted populations; Actin served as a loading control.

B. siRNA-transfected U87-MG/CD4/CXCR4 cells were treated or not with IFN for 24 h prior to infection with HIV-1 Renilla. Relative luminescence results for IFN-treated and -untreated conditions are shown. Multiple linear regression analysis.

C. DDX42 silencing efficiency measured by RT-qPCR (top) and immunoblot (bottom) in parallel samples from B.

D. DDX42-depleted cells were infected with HIV-1, and infection efficiency was measured by CA $p24^{Gag}$ intracellular staining and flow cytometry analysis. When indicated, cells were treated with azidothymidine (AZT) and lamivudine (3TC). Two-way ANOVA on log-transformed data with Dunnett's test.

E. siRNA-transfected MDMs were infected with a CCR5-tropic version of HIV-1 Renilla. Relative luminescence results from independent experiments performed with cells from three donors are shown. Two-way ANOVA on log-transformed data with Dunnett's test.

F. Primary CD4+ T cells were electroporated with Cas9-sgRNA RNPs using 2 non-targeting sgRNAs (sgCTRL1 and 2) and 5 sgRNAs targeting DDX42. Top: Cells were then infected with HIV-1 Renilla and relative infection efficiencies obtained with cells from three donors are shown. Two-way ANOVA on log-

188 transformed data with Dunnett's test. Bottom: DDX42 protein levels were determined by immunoblot, Actin
189 served as a loading control. A representative immunoblot is shown.
190 **G**. Firefly- or DDX42-expresssing U87-MG/CD4/CXCR4 cells were infected with HIV-1 Renilla. Relative
191 infection efficiencies are shown. Multiple linear regression analysis.
192 **A-G** Data represent the mean ± S.E.M of three independent experiments.
193

194 In order to confirm DDX42's effect on HIV-1 infection with an independent approach, we used
195 three different siRNAs to knockdown DDX42 expression. DDX42 depletion increased HIV-1
196 Renilla infection efficiency by 3 to 8-fold in U87-MG/CD4/CXCR4 cells, irrespectively of the
197 presence of IFN (Fig. 2B). Of note, DDX42 depletion was highly efficient (~90% efficiency both
198 at the mRNA and protein levels, Fig. 2C) but had no effect on cell viability (Fig. S2B).
199 Importantly, wild-type HIV-1 infection was also significantly impacted by DDX42 silencing, as
200 measured by Capsid (CA $p24^{Gag}$) intracellular staining 30 h post-infection in U87-
201 MG/CD4/CXCR4 cells (Fig. 2D). We then investigated whether DDX42 had an impact in HIV-1
202 primary target cells. In monocyte-derived macrophages (MDMs), we observed that HIV-1
203 infection was increased by about 2-fold following DDX42 silencing (Fig. 2E), whereas DDX42
204 mRNA abundance was decreased by only 40% (Fig. S2C). Electroporation of pre-assembled
205 Cas9-sgRNA ribonucleoprotein complexes (RNPs) was used to efficiently deplete DDX42 in
206 primary CD4+ T cells (Fig. 2F). DDX42 depletion increased HIV-1 infection by 2- to 3-fold,
207 showing a physiological role of DDX42 as an intrinsic inhibitor of HIV-1 in primary CD4+ T cells.
208 Next, we analysed the consequences of DDX42 overexpression on HIV-1 infection. An
209 irrelevant control (Firefly) or DDX42 were ectopically expressed in U87-MG/CD4/CXCR4 and
210 the cells were challenged with HIV-1 (Fig. 2G). DDX42 overexpression induced a substantial
211 inhibition of HIV-1 infection (~5-fold decrease in infection efficiency in comparison to the
212 control). Interestingly, the expression of K303E DDX42 mutant, which is unable to hydrolyse
213 ATP and may supposedly act as a dominant negative (25, 26), increased HIV-1 infection by 3-
214 fold (Fig. S2D), reminiscent of the impact of DDX42 depletion. Altogether, these data showed
215 that endogenous DDX42 is able to intrinsically inhibit HIV-1 infection.
216

217 In order to determine which step of HIV-1 life cycle was affected by DDX42, we quantified HIV-1
218 DNA accumulation over time in DDX42-silenced and control cells (Fig. 3A; silencing efficiency is
219 shown in Fig. 3B). DDX42 depletion increased accumulation of early and late reverse transcript
220 products (by 2.5- to 8-fold), as well as proviral DNA and 2-long terminal repeat (2-LTR) circles at
221 48h post-infection (by 2.5- to 4.5-fold). Importantly, DDX42 silencing did not impact HIV-1 entry
222 (Fig. S3A). These data suggested that endogenous DDX42 could inhibit reverse transcription
223 and/or impact genome stability, leading to a decrease in viral DNA accumulation. We
224 hypothesized that if that was the case, DDX42 should be found in close proximity to HIV-1
225 reverse transcription complexes during infection. In agreement with this, proximity ligation assay
226 (PLA) performed on HIV-1 infected MDMs showed that DDX42 was indeed in close vicinity of
227 Capsid (Fig. 3C).
228
229 We next examined the ability of DDX42 to inhibit infection by various primate lentiviruses,
230 including lab-adapted strains of HIV-1 (NL4-3, IIIB), transmitted/founder strains (27) (CH077.t,
231 CH106.c, REJO.c), HIV-2 and simian immunodeficiency virus from rhesus macaque (SIV_{MAC}).
232 DDX42 was depleted or not in TZM-bl reporter cells prior to infection with VSV-G-pseudotyped
233 lentiviruses, and infection efficiency was monitored 24h later (Fig. 3D; silencing efficiency is
234 shown in Fig. 3E). DDX42 depletion increased infection levels similarly with all the tested strains
235 of HIV-1 (i.e. 3- to 5-fold). HIV-2rod10 and SIV_{MAC} infection efficiencies were also slightly
236 improved in the absence of DDX42 (~2-fold). The analysis was then extended to two non-
237 primate lentiviruses, equine infectious anemia virus (EIAV) and feline immunodeficiency virus
238 (FIV), using GFP-coding LVs in U87-MG cells (Fig. 3F). DDX42 depletion appeared to increase
239 HIV-1, HIV-2 and FIV LV infection to the same extent (~2-fold), whereas EIAV infection was less
240 impacted. Of note, DDX42 antiviral activity appeared less potent on HIV-1 LVs compared to full-
241 length HIV-1, which might suggest that genome length or cis-acting elements could play a role
242 in DDX42 inhibition. We also observed that DDX42 depletion led to a significant increase in
243 infection with GFP-coding, MLV-derived vectors (Fig. 3G). These results strongly support a
244 general antiviral activity of DDX42 against retroviruses.

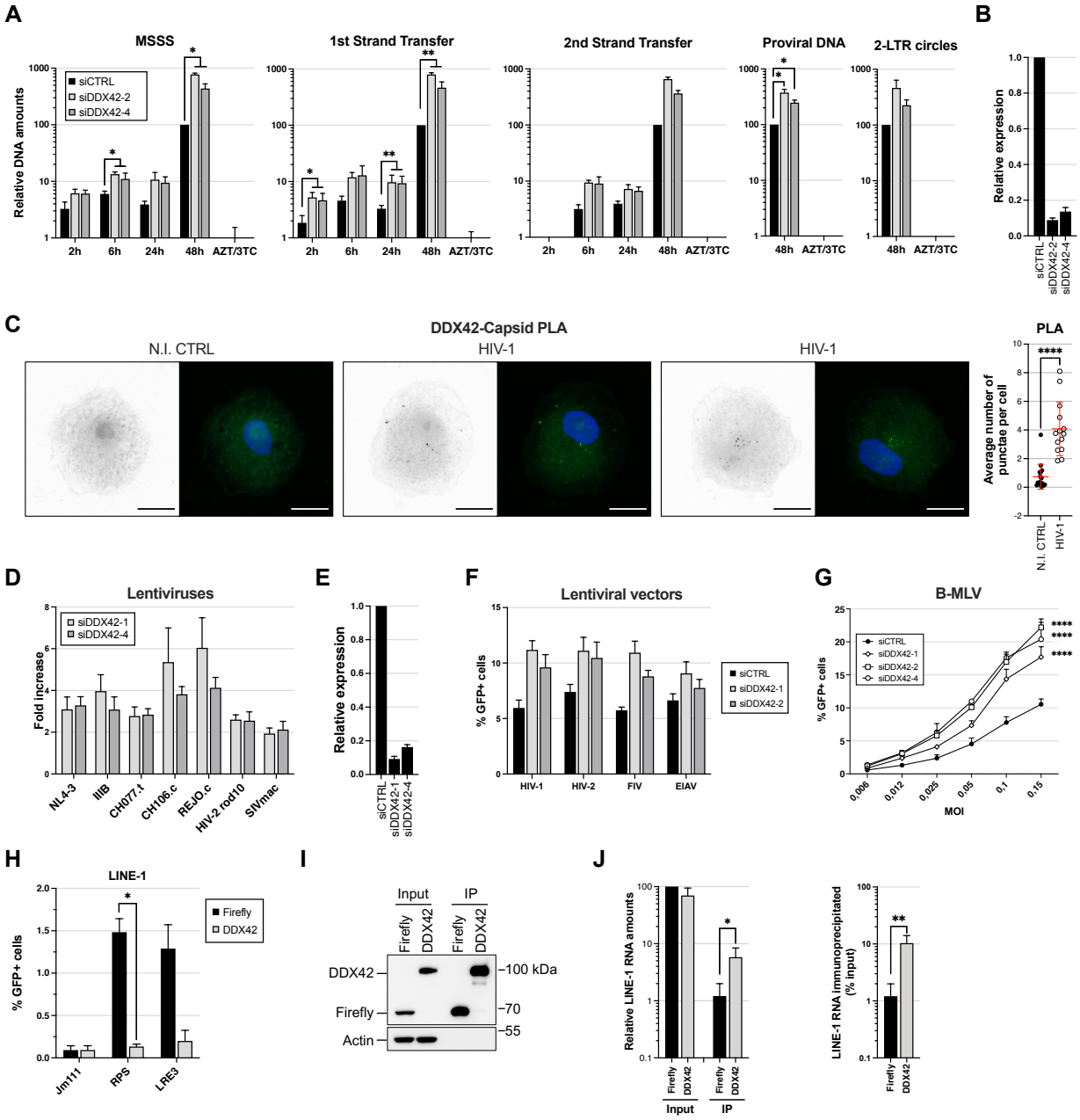

Figure 3. Characterization of DDX42 inhibitory activity against retroviruses and retroelements.

A. siRNA-transfected U87-MG/CD4/CXCR4 cells were infected with HIV-1 and relative amounts of Minus Strand Strong Stop (MSSS), 1st and 2nd Strand Transfer DNAs, and nuclear forms of HIV-1 DNA (proviral DNA, and 2-LTR circles) were quantified by qPCR. DNAs from cells infected for 48 h in the presence of AZT and 3TC were used as a control. Mixed-effects analysis on log-transformed data with Dunnett's test.

B. Silencing efficiency in parallel samples from A.

C. PLAs were performed in MDMs infected with HIV-1 or not (N.I. CTRL), using anti-Capsid and anti-DDX42 antibodies (nuclei stained with Hoechst). Images were acquired using a LSM880 Airyscan microscope. Left: representative images, scale-bar: 10 μm. Right: Average punctae quantified per cell in 3 independent assays done on MDMs from different donors with mean ± SD (n>65 cells per condition). Mann-Whitney test.

D. siRNA-transfected TZM-bl cells were infected and β-galactosidase signals measured 24 h later. The ratio of the signal in DDX42-depleted versus CTRL cells is shown.

E. Silencing efficiency in parallel samples from D.

259 **F.** siRNA-transfected U87-MG/CD4/CXCR4 cells were infected with HIV-1- HIV-2- FIV- EIAV-based, GFP-
260 coding LVs and infection efficiency was scored 24 h later by measuring the percentage of GFP expressing cells
261 by flow cytometry.
262 **G**. siRNA-transfected U87-MG/CD4/CXCR4 cells were infected with GFP-coding B-MLV and infection
263 efficiency measured 24h later by flow cytometry. Simple linear regression analysis.
264 **H**. HEK293T were co-transfected with GFP-coding LINE-1 plasmids (RPS-GFP or LRE3-GFP) or with an
265 inactive LINE-1 plasmid (JM111) together with either a Firefly- or DDX42-coding plasmid. GFP expression was
266 measured by flow cytometry 7 days later. Two-way ANOVA on log-transformed data with Sidak's test.
267 **I**. HEK293T were co-transfected with pRPS-GFP and a Flag-Firefly- (negative control) or Flag-DDX42-coding
268 plasmid, followed by Flag immunoprecipitation and immunoblot analysis. A representative immunoblot is
269 shown.
270 **J**. Left, RNA extraction and LINE-1 RT-qPCR on parallel samples from H. Two-way ANOVA on log-transformed
271 data with Sidak's test. Right, Percentage of immunoprecipitated RNA from I. T-test on log-transformed data.
272 **A-H**. Data represent the mean ± S.E.M of 3 independent experiments. **J**. Data represent the mean ± S.E.M of 5
273 independent experiments.
274

275 DDX42 can be found in the cytoplasm but is predominantly located in the nucleus in various cell
276 types, including monocyte-derived macrophages (28, 29) (Fig. S3B). Considering that DDX42
277 showed a broad activity against retroviruses and seemed to act at the level of reverse
278 transcription, we sought to investigate whether DDX42 could inhibit retrotransposons. Long
279 interspersed nuclear elements (LINE)-1 are non-LTR retrotransposons, which have been found
280 to be active in the germ line and some somatic cells (30). Interestingly, DDX42 was identified
281 among the suppressors of LINE-1 retrotransposition through a genome-wide screen in K562
282 cells, although not further characterized (31). To confirm that DDX42 could inhibit LINE-1
283 retrotransposition, HEK293T cells were co-transfected with GFP-expressing LINE-1 plasmids
284 (RPS or LRE3) or an inactive LINE-1 (JM111) together with a DDX42- or a control (Firefly)-
285 expressing plasmid (32). LINE-1 retrotransposition was quantified by flow cytometry 7 days later
286 (Fig. 3H). As the GFP cassette is cloned in antisense and disrupted by an intron, GFP is only
287 expressed after LINE-1 transcription, splicing, Orf2p-mediated reverse transcription, and
288 integration (32). Successful retrotransposition events were observed in >1.25% of control cells,
289 but in only <0.25% of DDX42-expressing cells (i.e. a percentage similar to what observed with
290 the non-active LINE-1), showing that DDX42 ectopic expression significantly suppressed LINE-1
291 retrotransposition. Next, we investigated whether DDX42 could physically interact with LINE-1

292 RNAs by performing cross-linking RNA immunoprecipitation. Cells were co-transfected with
293 GFP-expressing LINE-1 RPS plasmid and either flag-tagged-Firefly or -DDX42. Four days later,
294 the cells were treated with formaldehyde, lysed and the flagged proteins immunoprecipitated.
295 The immunoprecipitation eluates were then divided in two; the immunoprecipitated proteins
296 were analysed by immunoblot (Fig. 3I) and their associated RNAs were extracted and analysed
297 by RT-qPCR using LINE-1 specific primers (Fig. 3J). A significant enrichment of LINE-1 RNAs
298 was observed with DDX42 immunoprecipitation as compared to the Firefly negative control,
299 showing that DDX42 could interact with LINE-1 RNAs.
300
301 Finally, we sought to determine whether DDX42's inhibitory activity was specific towards
302 retroviruses and retroelements, or could be extended to other viruses, as observed for many
303 other anti-HIV-1 proteins, such as ZAP or BST-2/Tetherin (1, 8). To this aim, we tested the
304 impact of DDX42 depletion on nine RNA viruses from six different families: the orthomyxovirus
305 influenza A virus (IAV), the rhabdovirus vesicular stomatitis virus (VSV), the paramyxovirus
306 measles virus (MeV), the flaviviruses ZIKV, Dengue virus serotype 2 (DENV-2) and yellow fever
307 virus (YFV), the alphavirus CHIKV, the coronavirus SARS-CoV-2, which is responsible for the
308 current coronavirus disease (COVID)-19 pandemic, and the seasonal coronavirus HCoV-229E
309 (Fig. 4 and S4). Strikingly, DDX42 depletion had no significant effect on IAV, VSV and MeV
310 replication in U87-MG and Huh-7 cells, respectively (Fig. 4A-C; silencing efficiency is shown in
311 Fig. S4A), thereby strongly suggesting that manipulating DDX42 expression did not have a
312 broad and unspecific impact on target cells. Interestingly, depletion of endogenous DDX42 had
313 a modest but significant, positive impact on ZIKV in U87-MG cells (Fig. 4D), whereas the impact
314 in Huh-7 cells was minor (Fig. S4B and A), probably due to the fact that the silencing was less
315 efficient in the latter or, alternatively, that a wild-type version of ZIKV and a different readout was
316 used in this case. Similarly, DDX42 silencing had little effect on 2 other flaviviruses (DENV-2
317 and YFV) in Huh-7 cells, as measured by the number of cells positive for the viral protein E (Fig.
318 S4C-D). By contrast, DDX42 depletion had a profound effect on CHIKV (Fig. 4E), SARS-CoV-2
319 (Fig. 4F-G) and HCoV-229E (Fig 4SA and E) replication (up to 1 log-increase in infection

320 efficiency with CHIKV and HCoV-229, and 3 log-increase with SARS-CoV-2; silencing
321 efficiencies in the different cell lines used are shown in Fig. S4A). Plaque assays confirmed a
322 strong impact of DDX42 depletion on infectious SARS-CoV-2 production (Fig. 4G). In
323 agreement with this, DDX42 was recently identified as a potential inhibitor of SARS-CoV-2
324 replication in a whole-genome CRISPR screen in simian cells (33). Next, we used PLA to
325 determine whether DDX42 was in the vicinity of SARS-CoV-2 components in infected cells. To
326 this aim, PLA was performed with either an anti-double strand (ds)RNA or anti-Nucleoprotein
327 (N) antibody, together with an anti-DDX42 antibody, followed by immunofluorescence staining to
328 identify the infected cells (Fig. 4H-I). In the latter, there was a significantly higher number of
329 dsRNA-DDX42 and N-DDX42 PLA punctae than in control cells. This proximity suggested a
330 potential interaction between DDX42 and SARS-CoV-2 viral components. To test whether
331 DDX42 RNA helicase could indeed interact with viral RNAs, cross-linking RNA
332 immunoprecipitation experiments were conducted following viral infection of U87-MG cells
333 expressing either Flag-DDX42 or negative control Flag-Firefly (in addition to ACE2 for SARS-
334 CoV-2 infection). A significant enrichment of the viral RNAs recovered with Flag-DDX42 was
335 observed in comparison to the negative control. Importantly, such an enrichment was observed
336 for the sensitive viruses SARS-CoV-2 and CHIKV (Fig. 4J-K), but not for IAV, which was
337 insensitive to DDX42 antiviral activity (Fig. 4L and 4A).
338

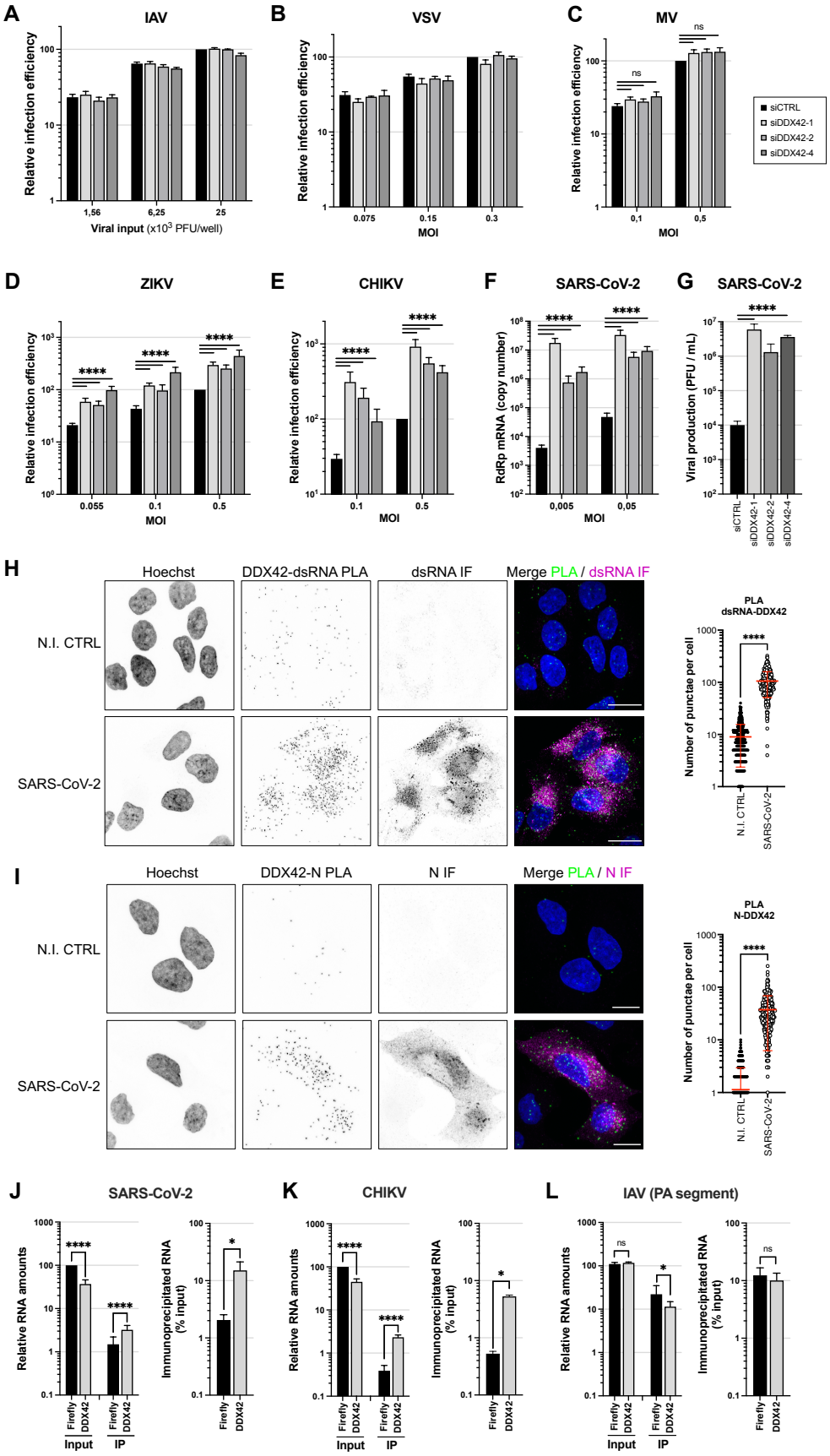

Figure 4. DDX42 exerts a broad antiviral activity on positive strand RNA viruses and interacts with viral RNAs from targeted viruses.

342 **A.** Relative IAV infection efficiency in siRNA-transfected U87-MG cells (Nanoluciferase activity 16 h post
343 infection).
344 **B.** Relative VSV infection efficiency in siRNA-transfected U87-MG cells (Firefly activity 24 h post infection).
345 **C.** Relative MeV infection efficiency in siRNA-transfected Huh-7 cells (GFP+ cells scored 24h post infection).
346 Multiple linear regression analysis.
347 **D.** Relative ZIKV infection efficiency in siRNA-transfected U87-MG cells (Nanoluciferase activity 24 h post
348 infection). Multiple linear regression analysis.
349 **E.** Relative CHIKV infection efficiency in siRNA-transfected U87-MG cells (Nanoluciferase activity 24 h post
350 infection). Multiple linear regression analysis.
351 **F.** Relative SARS-CoV-2 infection in siRNA-transfected A549-ACE2 cells (RdRp RT-qPCR 48 h post-
352 infection). Mixed-effects analysis on log-transformed data with Dunnett's test.
353 **G**. Viral production in cell supernatants from F (48 h post-infection, MOI 0,05) measured by plaque assays.
354 Two-way ANOVA on log-transformed data with Dunnett's test.
355 **H.** A549-ACE2 cells were infected or not with SARS-CoV-2 for 24 h prior to PLA using mouse anti-dsRNA (J2)
356 and rabbit anti-DDX42 antibodies, followed by additional immunofluorescence (IF) staining with anti-mouse
357 Alexa Fluor 546 antibody (PLA in green, IF in magenta). Representative Z-stack projection images are shown;
358 scale bar: 15 μm. Average punctae were quantified in 3 independent PLA assays with mean ± SD (n>75 cells
359 per condition). Mann-Whitney test.
360 **I**. Identical to H but using an anti-N antibody instead of anti-dsRNA antibody.
361 **J**. Left, Quantification of SARS-CoV-2 RNA by RT-qPCR in RNA from total U87-MG-ACE2 cell lysates (input)
362 and in Flag-Firefly (negative control) and Flag-DDX42 immunoprecipitation (IP). Multiple linear regression
363 analysis on log-transformed data. Right, Percentage of immunoprecipitated RNA. Paired t-test on log-
364 transformed data.
365 **K**. Identical to J following CHIKV infection of U87-MG cells.
366 **L**. Identical to J following IAV infection of U87-MG cells.
367 Data represent the mean ± S.E.M. of three (**A-E, J-L**), four (**F**) or two (**G**) independent experiments.
368

369 As mentioned above, DDX42's lack of effect on negative strand RNA viruses argued against a
370 global, indirect impact on the target cells. However, to confirm this, we performed RNA-seq
371 analysis on siRNA-treated U87-MG and A549-ACE2 cells. The results showed that DDX42
372 depletion didn't have a substantial impact on global cellular RNA expression (Supplementary
373 File 1 and Fig. S5). Of note, only 63 genes were commonly found differentially expressed upon
374 DDX42 depletion with the 3 different siRNAs in U87-MG cells, and only 23 differentially
375 expressed genes (DEGs) were identified in common in U87-MG and A549-ACE2 cells.
376 Importantly, no known restriction factors were identified among these DEGs (Supplementary
377 File 1). Taken together, these data strongly suggested that the DEAD-box RNA helicase DDX42
378 directly impacted viral replication, by interacting with viral RNAs.

379 **Discussion**

380

381 Here, we identified for the first time the RNA helicase DDX42 as an intrinsic inhibitor of HIV-1,
382 capable of limiting the efficiency of viral DNA accumulation. Moreover, our study revealed broad
383 activity of endogenous DDX42 against retroviruses and retroelements, which was observed in
384 various cell lines and primary cells, including primary CD4+ T cells. Strikingly, we observed that
385 DDX42 was able to inhibit viruses from other families, which possess different replication
386 strategies, including SARS-CoV-2 and CHIKV. However, DDX42 did not have an impact on all
387 the viruses we tested, as three different negative-strand RNA viruses were found insensitive to
388 DDX42 antiviral activity. This is reminiscent of other broad-spectrum antiviral inhibitors such as
389 MX1, which possesses some specificity despite being able to inhibit viruses from various
390 families (34). Further work is now warranted to explore in depth the breadth of DDX42 antiviral
391 activity and determine whether it is truly specific of positive strand RNA viruses.

392

393 Noteworthy, our PLA assays showed a close proximity between DDX42 and HIV-1 Capsid,
394 which is a viral protein recently shown to remain associated with reverse transcription
395 complexes until proviral DNA integration in the nucleus (35–37). We also observed a close
396 proximity between DDX42 and SARS-CoV-2 N or dsRNA, which could be suggestive of a
397 potential interaction of DDX42 with viral components. In line with this, LINE-1 RNAs, as well as
398 SARS-CoV-2 and CHIKV RNAs (but not IAV RNAs), were specifically pulled-down when DDX42
399 was immunoprecipitated. Taken together, these observations strongly suggest a direct mode of
400 action of DDX42, which could interact with target viral RNAs. Interestingly, DDX42 is known to
401 be a non-processive helicase, which also possesses RNA annealing activities and the ability to
402 displace RNA-binding proteins from single-stranded RNAs (23). Moreover, DDX42 binds to G-
403 quadruplexes (38), which are secondary structures found both in cellular and viral nucleic acids
404 and involved in various processes, such as transcription, translation and replication (39, 40).
405 The functional relevance of this ability to bind G-quadruplexes is currently unknown.
406 Interestingly, DDX42 was initially identified as a transient interactant of the spliceosome

407 component SF3b, and had been proposed to play a role in RNP remodeling in this context, but
408 this was not experimentally tested (41). Whether DDX42 actually plays a role in the splicing
409 machinery formation, or in any other cellular function(s), remains therefore to be assessed. A
410 better knowledge of DDX42 cellular functions may help understanding its mechanism of action
411 against viruses. Of note, the current known activities for DDX42 could be consistent with a
412 potential antiviral role through binding of viral secondary RNA structures and/or through viral
413 RNP remodeling (23, 42).
414
415 DEAD box RNA helicases are well-known to participate in innate immunity, with some of the
416 best examples being RIG-I-like receptors, which play an important role in viral nucleic acid
417 sensing (43). Additionally, some RNA helicases are involved in regulating (either positively or
418 negatively) innate immune signaling, while also being involved in various cellular functions. For
419 instance, DDX46 uses both its helicase and ATPase activities to catalyze conformational
420 changes and complex formation in the context of pre-spliceosome assembly (41, 44). Besides
421 this role, DDX46 was shown to negatively regulate innate immune activation by recruiting an
422 m6A eraser onto mRNAs coding key IFN signaling adaptors, such as MAVS, causing their
423 nuclear retention and decreasing IFN production (45). Other RNA helicases are well-known
424 inhibitors of viruses and/or retroelements, like MOV10 for instance. These RNA helicases can
425 generally be IFN-regulated (24). In contrast, there is very few known examples of RNA
426 helicases with antiviral effector activities, which would totally be IFN-independent. To our
427 knowledge, so far, in addition to DDX42, only DDX17 has been shown to possess intrinsic
428 antiviral functions. DDX17 is active against negative strand RNA bunyaviruses, through binding
429 of viral RNA secondary structures, and this activity seemed conserved in Drosophila and
430 humans (43). DDX17 and DDX42 are likely to ensure complementary functions by targeting
431 different viruses, through distinct RNA-binding specificities. Nevertheless, DDX42's broad
432 spectrum of action seems so far a unique feature among RNA helicases and further work is now
433 needed to understand the viral determinants for DDX42 restriction activity. While G-

434 quadruplexes could be preferential binding sites for DDX42 (23), viral genomes harbor
435 numerous highly structured elements that could also be involved.
436
437 In conclusion, this work shows for the first time an antiviral role for DDX42 and highlights the
438 importance of understanding the mechanism of action of this RNA helicase and how it may
439 participate in the control of positive-strand RNA virus replication. Such an understanding might
440 contribute to the development of future antiviral interventional strategies.
441

442 **Methods**

443

444 **Plasmids.** The pLentiCas9-Blast, pLentiGuide-Puro vectors and the GeCKO sub-library A and
445 B plasmids were a gift from Prof. F. Zhang (Addgene #52962, #52963, and #1000000048,
446 respectively (17)). LVs coding for sgRNAs targeting the candidate genes and control genes
447 were obtained by cloning annealed oligonucleotides in BsmBI-digested pLentiGuide-Puro, as
448 described (Addgene). Control sgRNAs and sgRNAs targeting the candidate genes, *MX2* and
449 *IFNAR1*, were designed with the Optimized CRISPR Design tool (not available anymore), or
450 with Chopchop (chopchop.cbu.uib.no). The sgRNA coding sequences used were as follow:
451 MX2 5'-CCGCCATTCGGCACAGTGCC-3', IFNAR1 5'-GACCCTAGTGCTCGTCGCCG-3',
452 sgCTRL-1 5'-AGCACGTAATGTCCGTGGAT-3', sgCTRL-2 5'-CAATCGGCGACGTTTTAAAT-
453 3', sgCTRL-3 5'-TTAATTTGGGTGGGCCCTGC-3', sgCTRL-4 5'-
454 TTGGATATTAATTAGACATG-3', sgDDX42-1 5'-TCCTGAACCACACCAGCAGT-3', sgDDX42-2
455 5'-GGTGGTCCTGGCACTAAGCG-3', sgDDX42-3 5'-AGGCACTGTGGGACTGCTGT-3'. All the
456 other sgRNA sequences are available upon request. In order to produce the HIV-1 based LVs
457 used to perform the different steps of the screen (pRRL.sin.cPPT.CMV/NeomycinR.WPRE,
458 pRRL.sin.cPPT.CMV/HygromycinR.WPRE and pRRL.sin.cPPT.CMV/ZeocinR.WPRE),
459 neomycin, hygromycin and zeocin resistance genes (i.e. the genes coding for Neomycin
460 phosphotransferase II, Hygromycin B phosphotransferase, and *Sh ble*) were amplified by PCR
461 from pcDNA3.1 (ThermoFisher Scientific), pAHM (11), and pcDNA3.1/Zeo (ThermoFisher
462 Scientific), respectively, and cloned by replacement of GFP in pRRL.sin.cPPT.CMV/GFP.WPRE
463 (46) using BamHI and SalI restriction sites. The pRRL.sin.cPPT.SFFV/E2-crimson-IRES-
464 PuromycinR.WPRE has been described (47). Human DDX42 cDNA was amplified by RT-PCR
465 using the SuperScript III™ (Invitrogen) from mRNAs of MDMs using primers DDX42-forward 5'-
466 AATTAATTTAGGATCCATGAACTGGAATAAAGGTGGTCCTG and DDX42-reverse 5'-
467 AATTAATTTACTCGAGCTAACTGTCCCATCGACTTTTCTTGCG, and cloned by replacement
468 of E2-crimson in BamHI-XhoI-digested pRRL.sin.cPPT.SFFV/E2crimson-IRES-
469 PuromycinR.WPRE, in order to obtain pRRL.sin.cPPT.SFFV/DDX42-IRES-PuromycinR.WPRE.

470 The pRRL.sin.cPPT.SFFV/CD4-IRES-CXCR4.WPRE was obtained by replacement of E2-
471 crimson-IRES-PuroR in pRRL.sin.cPPT.SFFV/E2-crimson-IRES-PuromycinR.WPRE with a
472 BamHI/SalI fragment digested CD4-IRES-CXCR4 PCR fragment obtained from pMLV-CD4-
473 IRES-CXCR4 (a gift from Prof. N. Sherer, Wisconsin University, USA).
474 pRRL.sin.cPPT.SFFV/Firefly-IRES-PuromycinR.WPRE was obtained by amplification of Firefly
475 by PCR from pGL4 (Promega) and cloned into BamHI-XhoI-digested pRRL.sin.cPPT.SFFV/E2-
476 crimson-IRES-PuromycinR.WPRE. In some experiments, LVs without a selection marker were
477 used: the IRES-PuromycinR cassette was removed by XhoI-SalI digestion and subsequent
478 ligation, to obtain pRRL.sin.cPPT.SFFV/Firefly.WPRE and
479 pRRL.sin.cPPT.SFFV/DDX42.WPRE. DDX42 K303E mutant was obtained by site-directed
480 mutagenesis (by overlapping PCR using the aforementioned DDX42-forward and -reverse
481 primers, respectively combined initially with reverse primer 5'-
482 GGCTGCAGTTTCCCCACTACCTGTTTTGGCAATACC and forward primer 5'-
483 GGTAGTGGGGAAACTGCAGCCTTCATTTGGCC). pRRL.sin.cPPT.SFFV/ACE2.WPRE has
484 been described (48) (Addgene 145842). Flag-DDX42 and Flag-Firefly were amplified by PCR
485 from the aforementioned LV plasmids and cloned into a NotI-XhoI-digested modified version of
486 pCAGGS (49) to obtain pCAGGS/flag-DDX42.WPRE and pCAGGS/flag-Firefly.WPRE. The
487 NL4-3/Nef–internal ribosome entry signal (IRES)-Renilla (NL4-3/Nef-IRES-Renilla) and the
488 CCR5-version of this proviral clone were gifts from Prof. Sumit Chanda (20). Wild-type and Ba-L
489 Env bearing HIV-1 NL4-3, IIIB and HIV-2 proviral clones have been described (50–52), as well
490 as the transmitted founder HIV-1 molecular clones CH077.t, CH106.c, REJO.c (gifts from Prof.
491 B. Hahn (27)) and HIV-2_{ROD10} and SIV_{MAC239} (53, 54). GFP-coding HIV-1 based LV system (i.e.
492 p8.91 HIV-1 Gag-Pol, pMD.G, and GFP-coding minigenome), and HIV-2, FIV, and EIAV-
493 derived, GFP coding LVs, as well as MLV-derived, GFP coding retroviral vectors have all been
494 described (55, 56, 57, 58). The LINE-1 plasmid 99 RPS-GFP PUR (pRPS-GFP), 99 RPS-GFP
495 JM111 PUR (pJM111) and pLRE3-GFP were developed by Prof. Kazazian's lab (32, 59, 60).
496

497 **Cell lines.** Human cell lines HEK293T, A549, U87-MG, TZM-bl were obtained from the ATCC
498 and the AIDS reagent program, respectively. T98G cells were a gift from Prof. G. Kochs
499 (Freiburg University, Germany), MDCK cells a gift from Prof. W. Barclay (Imperial College
500 London, UK), Vero E6 cells (Merck) were a gift from Christine Chable (CEMIPAI, CNRS),
501 respectively, Huh7.5.1 cells have been described (61), and the latter provided by Raphaël
502 Gaudin. Human hepatocellular carcinoma Huh-7 cells (62) were kindly given by Annette Martin
503 (Institut Pasteur, Paris). These cell lines were cultured in Dulbecco's Modified Eagle Medium
504 (DMEM) supplemented with 10% fetal bovine serum and 1 % penicillin-streptomycin
505 (Thermofisher). T98G/Cas9 and U87-MG/Cas9 were obtained by transduction of T98G and
506 U87-MG, respectively, with HIV-1-based LVs expressing the spCas9-P2A-Blasticidin cassette
507 (pLentiCas9-Blast (17)). U87-MG/CD4/CXCR4 have been described (11) and were further
508 modified to express Cas9 and Firefly using pLentiCas9-Blast and
509 pRRL.sin.cPPT.SFFV/Firefly.WPRE, respectively. T98G/Cas9/CD4/CXCR4/Firefly were
510 obtained by successive transductions of T98G/Cas9 with pRRL.sin.cPPT.SFFV/CD4-IRES-
511 CXCR4.WPRE at a high MOI, and pRRL.sin.cPPT.SFFV/Firefly.WPRE, at a low MOI,
512 respectively. Cell surface staining with anti-CD4 and CXCR4 antibodies (Miltenyi Biotec)
513 confirmed than more than 95% cells were positive for both markers. A549 cells stably
514 expressing ACE2 were generated by transduction with RRL.sin.cPPT.SFFV.ACE2.WPRE
515 containing-vector.
516 For antibiotic selection, cells were treated with 10 μg/mL Blasticidin (InvivoGen), 1 mg/mL
517 Zeocin (InvivoGen), 2 μg/mL Puromycin (Sigma-Aldrich), 250 μg/mL Hygromycin (Sigma-
518 Aldrich), 1 mg/mL G418 (Sigma-Aldrich). When indicated, universal type 1 IFN (PBL Interferon
519 Source) was added at 1000 U/mL for 16-24h prior to virus infection or RNA extraction, and AZT
520 and 3TC (AIDS reagent program) at 10 μM for 2 h prior to infection.
521
522 **Primary cells.** Blood from healthy donors was obtained from the Etablissement Français du
523 Sang, under agreement n°21PLER2019-0106. Peripheral blood mononuclear cells (PBMCs)

524 were isolated by centrifugation through a Ficoll® Paque Plus cushion (Sigma-Aldrich). Primary
525 human CD4+ T cells and monocytes were purified by positive selection using CD3 and CD14
526 MicroBeads, respectively (Miltenyi Biotec), as previously described (11). Monocytes were
527 incubated for 3 hours in serum-free Roswell Park Memorial Institute (RPMI) 1640 medium and
528 further differentiated into macrophages by culture for 5-7 days in RPMI 1640 supplemented with
529 10% fetal calf serum, 1% penicillin-streptomycin and 100 ng/ml granulocyte-macrophage
530 colony-stimulating factor (GM-CSF; Miltenyi). CD4+ T cells were cultured in RPMI
531 supplemented with 10% fetal bovine serum and 1% penicillin-streptomycin, and stimulated for
532 48h with 10 µg/ml phytohemagglutinin (PHA) (Fisher Scientific) and 50 U/mL interleukin-2 (IL-2,
533 Miltenyi Biotec) prior to electroporation.
534
535 **Genome-scale CRISPR/Cas9 screens**. The plasmids coding GeCKO sub-libraries A and B
536 were amplified and prepared according to the provided guidelines (Lentiviral Crispr Toolbox,
537 Addgene). 60 million T98G/Cas9 cells were transduced with GeCKO LVs at a MOI of 0,1 to
538 cover about 100-times the half-library complexity. After 48h, the cells were selected with
539 puromycin, amplified for 12-15 days. 45 million cells were harvested and frozen down at -80°C
540 for subsequent genomic DNA extraction, using the QIAamp DNA Blood Maxi Kit according to
541 manufacturer's instructions (Qiagen). In parallel, 60 million cells from the initial GeCKO
542 populations were used for the screen. The cells were treated with 1000 U/mL IFN for 24h,
543 infected with LVs coding a hygromycin resistance cassette. 48h later the cells selected with
544 hygromycin and the surviving cells amplified. Two other rounds of IFN treatment, LV infection
545 and antibiotic selection were subsequently performed with LVs coding a neomycin resistance
546 cassette and a zeocin resistance cassette, respectively. The three time-selected populations
547 were amplified and 45 million cells were harvested and stored at -80°C for subsequent genomic
548 DNA extraction, as previously. After genomic DNA extraction, the sgRNA coding sequences
549 integrated in the genomic DNA from the initial and 3-times selected populations were amplified
550 by touch-down PCR and sequenced by Illumina deep sequencing. To this aim, 120 µg of
551 genomic DNA was amplified using DNA Herculase II Fusion DNA polymerase (Agilent) in the

552 presence of 2% DMSO, 1 mM of dNTPs; and 400 nM of the following primers: Forward-primer1:
553 5'-TCGTCGGCAGCGTCAGATGTGTATAAGAGACAGCTTGTGGAAAGGACGAAACACC-3' for
554 screen A or Forward-primer2: 5'-
555 TCGTCGGCAGCGTCAGATGTGTATAAGAGACAGGATCTTGTGGAAAGGACGAAACACC-3'
556 used for screen B, together with reverse primer: 5'-
557 GTCTCGTGGGCTCGGAGATGTGTATAAGAGACAAAGGTCCATTAGCTGCAAAGATTCCTCT
558 C-3'). Briefly, after 5 minutes at 95°C, 14 cycles of pre-amplification were performed with a
559 hybridization temperature decreasing by 0.5°C per cycle (30 sec at 95°C, 30 sec at 60°C, 30
560 sec at 72°C), followed by 30 cycles of amplification (30 sec at 95°C, 30 sec at 53°C, 30 sec at
561 72°C). 50 ng of each amplicon was dual indexed in a 5-cycle PCR reaction using the PCR
562 module and indexed primers from the Nextera kit (Illumina). Resulting libraries were purified on
563 AMPure XP magnetic beads (Beckman Coulter) using a 0,8X ratio and verified on Fragment
564 Analyzer using the HS NGS fragment kit (Agilent). Libraries were quantified using
565 microfluorimetry (QuBit, Invitrogen), mixed with a PhiX library (Illumina) and sequenced on one
566 single read 50nt lane of Hiseq2500 using the rapid mode.
567 Image analyses and base calling were performed using the Illumina HiSeq Control Software and
568 Real-Time Analysis component (v1.18.66.3). Demultiplexing was performed using Illumina's
569 conversion software (bcl2fastq 2.20). The quality of the raw data was assessed using FastQC
570 (v0.11.5) from the Babraham Institute and the Illumina software SAV (Sequencing Analysis
571 Viewer). Potential contaminants were investigated with the FastQ Screen(63) (v0.11.4) software
572 from the Babraham Institute.
573 Sequencing reads were trimmed using Cutadapt (64) (v1.13), with options -g [primer sequence]
574 -u [length of remaining 3' bases] -e 0.2 -m 18 -l 20, to remove primer sequences and retrieve
575 the 20 bases long sequences corresponding to sgRNAs. These retrieved sequences were then
576 aligned to the GecKOv2 Human Library (A or B) reference sequences (keeping only non-
577 duplicated sgRNA sequences, the duplicated ones being annotated) using Bowtie (65) (v1.2),
578 with options -v 2 -norc -S. Resulting bam files were sorted and indexed using Samtools (66)
579 (v1.5). Quantification of sgRNAs was done using Samtools idxstats. MAGeCK (18) (v0.5.7) was

580 used to normalize (total count method) and identify enriched sgRNAs and genes in 3-times
581 selected cell populations versus starting GeCKO transduced cells (mageck test command).
582
583 **Lentiviral and retroviral production.** To produce lentiviral vector particles, HEK293T cells
584 were transfected by polyethylenimine (PEI) co-transfection with miniviral, HIV-1 based genome
585 coding plasmids (e.g. LentiCas9-Blast, LentiGuide-Puro or pRRL-SFFV), p8.91 (HIV-1 GagPol)
586 and pMD.G (VSV-G) at a ratio of 1:1:0.5, respectively. The medium was replaced after 6h and
587 viral particles were harvested 42h later, filtered, and directly used to transduce target cells (or
588 stored at -80°C). After 4 to 6 hours, the transduction medium was replaced with complete
589 DMEM, and the cells were treated 48h later with the relevant antibiotics. The HIV-2-, FIV-,
590 EIAV-GFP coding LVs were produced using GFP-coding HIV-2-, FIV-, EIAV-based miniviral
591 genomes, together with HIV-2-, FIV-, EIAV- GagPol, expression constructs and pMD.G at a
592 ratio of 1:1:0.5. MIGR1 MLV-derived retroviral vectors were obtained with B-MLV Gag-Pol-
593 expressing plasmid pCIG3B, the GFP-expressing minigenome pMIGR1 and pMD.G. at a ratio
594 of 1:1:0.5, respectively and harvested as previously described.
595 HIV-1 Renilla and NL4-3 HIV-1 were produced by standard PEI transfection of HEK293T. When
596 indicated, pMD.G was cotransfected with the provirus at a 3:1 ratio. The culture medium was
597 changed 6h later, and virus-containing supernatants were harvested 42h later. Viral particles
598 were filtered, purified by ultracentrifugation through a sucrose cushion (25% weight/volume in
599 Tris-NaCl-EDTA buffer) for 75 min at 4°C and 28,000 rpm using a SW 32 TI rotor (Beckman
600 Coulter), resuspended in serum-free RPMI 1640 or DMEM medium and stored in small aliquots
601 at -80°C. Viral particles were titrated using an HIV-1 $p24^{Gag}$ Alpha-Lisa kit and an Envision plate
602 reader (Perkin Elmer) and/or by determining their infection titers on target cells.
603
604 **Lentiviral and retroviral infections.** For infections with replication-competent HIV-1 Renilla or
605 wild-type and/or VSV-G pseudotyped-HIV-1, target cells were plated at 2.5 x 10^4 cells per well
606 in 96-well plates or at 2 x 10^5 cells per well in 12-well plates and infected for 24-48 h before lysis
607 and Renilla (and Firefly) luciferase activity measure (Dual-Luciferase® Reporter Assay System

608 Promega) or fixation with 2% paraformaldehyde (PFA)-PBS, permeabilization (Perm/Wash
609 buffer, BDBiosciences) and intracellular staining with the anti-p24^{Gag} KC57-FITC antibody
610 (Beckman Coulter), as described previously (67). For TZM-bl assays, the β-galactosidase
611 activity was measured using the Galacto-Star™ system (ThermoFisher Scientific). For infections
612 with lentiviral and retroviral vectors, target cells were plated at 2.5 x 10^4 cells per well in 96-well
613 plates the day prior to infection with vectors at the indicated MOIs, and the percentages of
614 infected cells were scored by flow cytometry 24h later. For primary CD4+ T cell infections, 10^5
615 cells were infected with 100 ng p24^{Gag} of HIV-1 Renilla for 24 h prior to lysis and luciferase
616 activity measure. For MDM infections, 8 x 10^4 cells were infected with 100 ng p24^{Gag} of a CCR5-
617 tropic version of HIV-1 Renilla for 30 h prior to lysis and luciferase activity measure.
618
619 **Retrotransposon assays.** For GFP-based retrotransposon assays, HEK293T cells (2 x 10^5
620 cells) were co-transfected with either 1 µg of pJM111 (a negative control with two point
621 mutations in ORF1 that abolish retrotransposition), pRPS-GFP or pLRE3-GFP with either 1 µg
622 of pCAGGS-Flag-Firefly or pCAGGS-Flag-DDX42. At 7 days post-transfection, the percentage
623 of GFP-expressing cells was scored by flow cytometry.
624
625 **CRISPR/Cas9 knock-out.** For CRISPR/Cas9 knock-out in cell lines, Lentiguide-Puro LVs
626 coding sgRNAs targeting the indicated genes or non-targeting sgRNAs were produced, and
627 U87-MG Cas9/CD4/CXCR4/Firefly were transduced for 6 h before replacing the supernatants
628 with fresh, complete medium. The transduced cells were selected with puromycin two days later
629 and amplified for 12-15 days. For CRISPR/Cas9 knock-out in activated primary CD4+ T cells, 2
630 million cells per condition were washed with PBS1X, and electroporated using the 4d-
631 Nucleofector® (Lonza) and the Amaxa P3 primary cell kit with 183 pmol of crispr/tracr RNA
632 duplex (Alt-R CRISPR-Cas9 crRNA XT and tracrRNA XT, IDT®) and 61 pmol of Cas9 (Alt-R®
633 S.p. Cas9 Nuclease V3, IDT®). After electroporation, the cells were incubated for 4 days at
634 37°C in X-VIVO15 medium (Lonza) supplemented with 1% pen/strep and IL-2 at 500 U/ml prior
635 to cell counting and infection. The crRNA sequences of the sgDDX42-1, -2, and -3 were

636 identical to the ones cloned in pLentiguide-Puro, and the crRNA of the sgDDX42-4 and
637 sgDDX42-5 were pre-designed by IDT®, as follow: sg4-DDX42 5'-
638 CGGAGATCTATTAACTGCTG-3', sg5-DDX42 5'-GAGTTGGTGAGTTTTCAGC-3'.
639
640 **siRNA transfection.** DDX42 and control knockdowns were achieved by transfecting the
641 indicated siRNAs at 44nM, 14.2nM, and 100nM final in U87-MG and Huh-7 cells, TZM-bl cells
642 and MDMs, respectively, with lipofectamine RNAimax (Thermofisher Scientific) according to the
643 manufacturer's instructions. The scramble siRNA controls used were universal siCTRL1
644 (SIC001) and siCTRL2 (SIC002) (Sigma-Aldrich) and the sequences of the siRNAs targeting
645 DDX42 were siDDX42-1: 5'-CAGAAUGCCUGGUUUCGGA-3' (SASI_Hs01_00119846, Sigma-
646 Aldrich®), siDDX42-2: 5'-CUUACCUUGUGUUUGAUGA-3' (SASI_Hs01_00119845, Sigma-
647 Aldrich®), siDDX42-4: 5'-AUCUCGAAUACCCUUUACG-3' (ID :136410, Ambion®).
648
649 **Cross-linking RNA immunoprecipitation.** For LINE-1 RNA immunoprecipitation, HEK293T
650 cells were co-transfected with equal amounts of pRPS-GFP and pCAGGS-Flag-DDX42 or -
651 Flag-Firefly. For viral RNA immunoprecipitation, U87-MG cells were transduced with either Flag-
652 Firefly or Flag-DDX42 coding lentiviral vectors (pRRL.sin.cPPT.SFFV/Flag-Firefly.WPRE and
653 pRRL.sin.cPPT.SFFV/Flag-DDX42.WPRE, respectively) and infected with CHIKV at MOI 0.1,
654 SARS-CoV-2 at MOI 0.13, or A/Victoria/3/75 IAV at MOI 0.1 for 24 h. 4 days post LINE-1-
655 transfection or 24 h post-infection, cells were washed twice in PBS1X, incubated for 10 min with
656 0,1% formaldehyde in PBS1X, for 5 min in 250 mM Glycine and washed twice in cold PBS1X.
657 Cells were lysed in RIPA buffer (50 mM Tris/HCl pH 7.5, 150 mM NaCl, 1% NP-40, 0.5%
658 sodium deoxycholate, 1 mM EDTA, protease inhibitor cocktail and 40 U/mL RNasin). The
659 lysates were clarified by centrifugation at 16,000*g*, for 10 min at 4 °C. Fractions of cell lysates
660 were harvested at this stage to serve as controls for protein and RNA inputs (15%) and the rest
661 was incubated with Flag-magnetic beads (ThermoFisher Scientific) for 2 h at 4 °C. The beads
662 were washed 5 times in RIPA buffer and the immunoprecipitated proteins eluted using 150
663 µg/mL 3x Flag peptide (Sigma-Aldrich) in elution buffer (50 mM Tris/HCl pH 7.5, 75 mM NaCl,

664 1mM DTT, protease inhibitor cocktail and 40 U/mL RNasin) for 2 h. Fractions of eluates were
665 harvested for immunoblot analysis (1/6th) and the rest subjected to RNA extraction (5/6th). RNA
666 extractions were then performed using TRIzol (ThermoFisher Scientific).
667
668 **RNA quantification by RT-qPCR.** To check silencing efficiency or measure gene induction
669 after IFN treatment, 0,5-2 x 10^6 cells were collected 2-3 days after siRNA transfection or 24h
670 after IFN treatment or no treatment, and total RNAs were isolated using the RNeasy kit with on-
671 column DNase treatment (Qiagen). cDNAs were generated using 250 ng RNA (High-Capacity
672 cDNA Reverse Transcription Kit, Applied Biosystem, ThermoFisher Scientific, catalogue number
673 4368814) and analysed by quantitative (q)PCR using TaqMan gene expression assays (Applied
674 Biosystem) specific for ACTB (Hs99999903_m1), GAPDH (Hs99999905_m1), and DDX42
675 (Hs00201296_m1). Triplicate reactions were run according to the manufacturer's instructions
676 using a ViiA 7 Real-Time PCR system. For relative quantification, samples were normalized to
677 both ACTB and GAPDH mRNA expression and ΔΔCt analysis was performed.
678 For the measure of LINE-1 RNAs, 100 ng RNA (from cell extracts) or 25 μl of RNA extracted
679 from the IP eluates (i.e. ~60% of the total amount of immunoprecipitated RNA) were reverse
680 transcribed and analysed by qPCR using primers and probe specific for *ORF2*: ORF2-forward
681 5'-CACCAGTTAGAATGGCAATCATTAAA-3', ORF2-reverse 5'-
682 GGGATGGCTGGGTCAAATGG-3' with ORF2-probe 5'-[FAM]-
683 AGGAAACAACAGGTGCTGGAGAGGATGC-[TAMRA]-3. Absolute quantification was
684 performed using a pRPS-GFP standard curve.
685 For the measure of SARS-CoV-2 replication, 3 x 10^5 cells were harvested and total RNA was
686 extracted using the RNeasy kit (Qiagen) employing on-column DNase treatment. 125 ng of
687 cellular RNAs were used to generate cDNAs that were analysed by qPCR using RdRp primers
688 and probe, as follow: RdRp_for 5'-GTGARATGGTCATGTGTGGCGG-3', RdRp_rev 5'-
689 CAAATGTTAAAAACACTATTAGCATA-3', and RdRp_probe 5'-[FAM]-
690 CAGGTGGAACCTCATCAGGAGATGC-[TAMRA]-3' (68). pRdRp (which contains an RdRp
691 fragment amplified from SARS-CoV-2-infected cell RNAs (48)) was diluted in 20 ng/ml salmon

692 sperm DNA to generate a standard curve to calculate relative cDNA copy numbers and confirm
693 the assay linearity (detection limit: 10 molecules of RdRp per reaction).
694 For the measure of the amounts of viral RNAs in the RNA immunoprecipitation experiments,
695 100 ng RNA from cell lysates (input) or 25 µl of RNA extracted from the IP eluates (i.e. ~60% of
696 the total amount of immunoprecipitated) were reverse transcribed using the High-Capacity
697 cDNA Reverse Transcription Kit as above. For SARS-CoV-2, the cDNAs were analysed by
698 RdRp RT-qPCR. For CHIKV RNA, the following primers and probe were used for the qPCR
699 reactions: E1-C21-forward 5'-ACGCAGTTGAGCGAAGCAC-3', E1-C21-reverse 5'-
700 CTGAAGACATTGGCCCCAC-3' (69), and E1-C21-probe 5'-[FAM]-
701 CTCATACCGCATCTGCATCAGCTAAGCTCC-[TAMRA]-3'. pE1 (which contains an E1
702 fragment amplified from CHIKV-infected cell RNAs using primers E1-C21 forward and E1-C21
703 reverse and cloned into pPCR-Blunt II-TOPO) was used to generate a standard curve and
704 ensure the linearity of the assay (detection limit: at least 10 molecules per reaction). For
705 A/Victoria/3/75 IAV RNA, the following primers and probe, specific for the PA segment, were
706 used, as follow: PA-forward 5'-TTGCTGCACAGGATGCATTA-3', PA-reverse 5'-
707 AGATTGGAGAAGACGTGGCT-3' and PA-probe 5'-[FAM]-
708 TGGCTCTGCAATGGGACACCTCTGC-[TAMRA]-3'. pPolI-RT-Victoria-PA (70) was used to
709 generate a standard curve and ensure the linearity of the assay (detection limit: at least 10
710 molecules per reaction).
711
712 **Quantification of HIV-1 DNAs.** To measure HIV-1 cDNAs, 2 x 10^5 cells transfected with a
713 control siRNA or siRNAs targeting DDX42 were plated in 24-well plates, and treated or not with
714 10 µM AZT and 3TC 1-2 h prior to infection. The cells were infected with NL4-3 HIV-1 (60 ng
715 $p24^{Gag}$) for 2 h at 37°C, washed with PBS1X and incubated in complete DMEM before being
716 harvested at the indicated times. Cell pellets were frozen at -80°C after two washes in PBS1X.
717 Total DNA extraction was performed using the DNeasy kit (Qiagen) according to the
718 manufacturer's instructions, and a DpnI-treatment step was performed prior to qPCR. Strong
719 stop reverse transcription products were detected using forward primer oHC64 5'-

720 TAACTAGGGAACCCACTGC-3' and reverse primer oHC65 5'-GCTAGAGATTTTCCACACTG-
721 3', 2nd strand transfer product using oHC64 and oSA63R 5'-
722 CTGCGTCGAGAGATCTCCTCTGGCT-3', together with oHC66 probe 5'-[FAM]-
723 ACACAACAGACGGGCACACACTA-[TAMRA]-3'. 2-LTR circular forms were detected using
724 2LTR-forward 5'-GTAACTAGAGATCCCTCAG-3' and 2LTR-reverse 5'-
725 TGGCCCTGGTGTGTAGTTC-3' together with 2LTR-probe 5′-[FAM]-
726 CTACCACACACAAGGCTACTTCCCTGAT-[TAMRA]-3'. Integrated viral DNA was analysed
727 using an Alu qPCR as described before (11). Briefly, a preamplification of 16 cycles was
728 performed (15 sec at 94°C, 15 sec at 55°C, 100 sec at 68°C) with Platinum Taq DNA High
729 Fidelity polymerase (Invitrogen) using 100 nM of genomic Alu forward primer 5′-
730 GCCTCCCAAAGTGCTGGGATTACAG and 600 nM of U3-reverse primer 5'-
731 CTTCTACCTTATCTGGCTCAAC-3'. The pre-amplification step was performed on serial
732 dilutions of all the DNA samples, as well as of a positive control (total DNA from U87-MG
733 infected with a high input of NL4-3), to ensure the linearity of the assay. Background levels were
734 assessed using linear, one-way amplification by performing the pre-amplification PCR with the
735 U3-reverse primer alone. Then a qPCR was performed on pre-amplification products using U3-
736 forward primer 5'-TCTACCACACACAAGGCTAC-3' and U3-reverse primer with the U3 probe
737 5'-[FAM]-CAGAACTACACACCAGGGCCAGGGGTCA-[TAMRA]-3'. qPCR reactions were
738 performed in triplicates, in Universal PCR master mix using 900nM each primer and 250nM
739 probe with the following program: 10 min at 95°C followed by 40 cycles (15 sec at 95°C and 1
740 min at 60°C). pNL4-3 or pTOPO-2LTR (generated by pTOPO cloning of a 2-LTR circle junction
741 amplified from NL4-3 infected cells, using oHC64 and U3-reverse primers into pCR™2.1-
742 TOPO™) were diluted in 20 ng/ml of salmon sperm DNA to create dilution standards used to
743 quantify relative cDNA copy numbers and confirm the linearity of all assays.
744
745 **Proximity Ligation assays (PLAs).** The proximity ligation assays were performed using the
746 Duolink® in situ Detection Reagents (Sigma-Aldrich, DUO92014). For PLA with HIV-1, MDMs
747 were plated in 24-well plates with coverslips pre-treated with poly-L-lysin (Sigma-Aldrich) and

748 infected with 1 μg $p24^{Gag}$ of HIV-1 NL4-3 (Ba-L Env) or mock-infected. For PLA with SARS-CoV-
749 2, A549-ACE2 cells were plated in 24-well plates with coverslips and infected at an MOI of 0,1.
750 24 h later, the cells were fixed with 2-4% paraformaldehyde in PBS1X for 10 min, washed in
751 PBS1X and permeabilized with 0.2% Triton X-100 for 10 min. After a couple of washes in
752 PBS1X, either NGB buffer (50 mM NH_4Cl, 2% goat serum and 2% bovine serum albumin in
753 PBS) or Duolink® blocking solution was added for 1h. Cells were incubated with mouse AG3.0
754 anti-HIV-1 Capsid antibody (National Institutes of Health (NIH) AIDS Reagent Program #4121),
755 or J2 anti-dsRNA antibody (SCICONS), or anti-SARS-CoV-2 Nucleoprotein (N; BioVision), and
756 rabbit anti-DDX42 antibody (HPA023571, Sigma-Aldrich) diluted in NGB buffer or in Duolink®
757 blocking solution for 1h. After 2 washes in PBS1X, the cells were incubated with the DUOLINK®
758 in situ PLA® Probe Anti-rabbit minus (DUO92006) and DUOLINK® in situ PLA® Probe Anti-
759 mouse plus (DUO92001) for 1h at 37°C. After 2 washes in PBS1X, the ligation mix was added
760 for 30 min at 37°C. After 2 washes in PBS1X, the cells were incubated with the amplification mix
761 for 100 min at 37°C followed by 3 washes in PBS1X. In the case of SARS-CoV-2 infection, an
762 additional staining was performed by incubating cells in an anti-mouse Alexa Fluor secondary
763 antibody. Finally, the cells were washed twice with PBS1X and stained with Hoechst at 1 μg/mL
764 for 5 min, washed again and the coverslips mounted on slides in Prolong mounting media
765 (ThermoFisher Scientific). Z-stack images were acquired using an LSM 880 confocal
766 microscope (ZEISS) using a 63x lens. PLA punctae quantification was performed using the FIJI
767 software (71). Briefly, maximum z-projections were performed on each z-stack and the number
768 of nuclei per field were quantified. Then, by using a median filter and thresholding, PLA punctae
769 were isolated and quantified automatically using the Analyse Particles function. To obtain a
770 mean number of dots per cell, the number of PLA dots per field were averaged by the number
771 of nuclei. In the case of SARS-CoV-2 infection, the infected cells were identified using N or
772 dsRNA immunofluorescence staining. For representative images, single cells were imaged
773 using a LSM880 confocal microscope coupled with an Airyscan module. Processing of the raw
774 Airyscan images was performed on the ZEN Black software.
775

776 **Immunoblot analysis.** Cell pellets were lysed in sample buffer (200 mM Tris-HCl, pH 6.8, 5.2%
777 SDS, 20% glycerol, 0.1% bromophenol blue, 5% β-mercaptoethanol), resolved by SDS–PAGE
778 and analysed by immunoblotting using primary antibodies specific for human DDX42
779 (HPA023571, Sigma-Aldrich), Flag (M2, Sigma-Aldrich) and Actin (A1978, Sigma-Aldrich),
780 followed by secondary horseradish peroxidase-conjugated anti-mouse or anti-rabbit
781 immunoglobulin antibodies and chemiluminescence (Bio-Rad). Images were acquired on a
782 ChemiDoc™ gel imaging system (Bio-Rad).
783
784 **IAV production and infection.** We have described previously IAV NanoLuciferase reporter
785 virus generation (47). Stocks were titrated by plaque assays on MDCK cells. IAV challenges
786 were performed in serum-free DMEM for 1 h and the medium was subsequently replaced with
787 DMEM containing 10%. IAV infection experiments were performed in triplicates in 96-well
788 plates with cultures maintained for 16 h post-challenge. NanoLuciferase activity was measured
789 with the Nano-Glo assay system (Promega), and luminescence was detected using a plate
790 reader (Infinite® 200 PRO, Tecan).
791
792 **VSV production and infection.** A VSV-G pseudotyped-VSV-Δenv reporter virus, coding both
793 GFP and Firefly Luciferase, was obtained from Gert Zimmer . The virus was amplified on
794 pMD.G transfected HEK293T and titrated thanks to the GFP reporter gene. For infection, 2.5 x
795 10^4 cells per well in 96-well plates were infected at the indicated MOIs. 24h after infection, cells
796 were lysed and Firefly luciferase activity was measured (Firefly luciferase Assay System
797 Promega).
798
799 **Measles virus production and infection.** Measles virus GFP strain (MeV-GFP), which was
800 kindly provided by F. Tangy (Institut Pasteur, Paris), was previously described (73). Viral stocks
801 were produced on Vero NK cells. After 4 days of infection, supernatant was collected and then
802 centrifugated to eliminate dead cells or fragments. Stocks were tittered using median tissue
803 culture infectious dose assays ($TCID_{50}$) on Vero NK cells. Cells were infected with 10-fold serial

804 dilutions of viral stocks and incubated for 7 days. Cells were then washed with PSB and fixed
805 with 3% formaldehyde crystal violet during 30 min and finally rinsed with water. For infections,
806 Huh-7 cells were infected at the indicated multiplicity of infection (MOI) in DMEM without FBS
807 for 2 h in small volume of medium to enhance contacts with the inoculum and the cells. After 2
808 h, the viral inoculum was replaced with fresh DMEM 10% FBS 1% P/S. 24 h post-infection the
809 cells were harvested and samples separated in half for Western blot and flow cytometry
810 analysis.
811
812 **ZIKV production and infection.** The nanoluciferase expressing ZIKV construct has been
813 described (74). The corresponding linearized plasmid was transcribed in vitro using the
814 mMESSAGE mMACHINE™ SP6 transcription kit (Thermofischer Scientific) and HEK293T cells
815 were transfected with the transcribed RNA. After 7 days, supernatants were harvested, filtered
816 and stock titers were determined by plaque assays on Vero cells. For infections, 2.5 x 10^4 cells
817 per well in 96-well plates were infected, at the indicated MOIs. 24h after infection, cells were
818 lysed and Nanoluciferase activity was measured using the Kit Nano Glo luciferase Assay
819 (Promega).
820
821 **CHIKV production and infection.** The Nanoluciferase luciferase coding CHIKV construct was
822 a gift from Andres Merits. The linearized plasmid coding CHIKV genome was transcribed with
823 the mMESSAGE mMACHINE SP6 kit (Thermofischer Scientific) and 5 x 10^5 HEK293T were
824 transfected with 1-4 μg of transcribed RNA, using Lipofectamine 2000 (Thermofischer
825 Scientific). After 24h, supernatants were harvested, filtered and viruses were then amplified on
826 baby hamster kidney (BHK21) cells. Stock titers were determined by plaque assays on Vero
827 cells. For infections, 2.5 x 10^4 cells per well in 96-well plates were infected at the indicated
828 MOIs. 24h after infection, cells were lysed and Nanoluciferase activity was measured.
829
830 **SARS-CoV-2 production and infection.** The SARS-CoV-2 BetaCoV/France/IDF0372/2020
831 isolate was supplied by Pr. Sylvie van der Werf and the National Reference Centre for

832 Respiratory Viruses hosted by Institut Pasteur (Paris, France). The patient sample from which
833 strain BetaCoV/France/IDF0372/2020 was isolated was provided by Dr. X. Lescure and Pr. Y.
834 Yazdanpanah from the Bichat Hospital, Paris, France. The virus was amplified in Vero E6 cells
835 (MOI 0,005) in serum-free media supplemented with 0,1 μg/ml L-1-p-Tosylamino-2-phenylethyl
836 chloromethylketone (TPCK)-treated trypsin (Sigma-Aldrich). The supernatant was harvested at
837 72 h post infection when cytopathic effects were observed (with around 50% cell death), cell
838 debris were removed by centrifugation, and aliquots stored at -80C. Viral supernatants were
839 titrated by plaque assays in Vero E6 cells. Typical titers were 5.10^6 plaque forming units
840 (PFU)/ml. Infections of A549-ACE2 cells were performed at the indicated multiplicity of infection
841 (MOI; as calculated from titers obtained in Vero E6 cells) in serum-free DMEM and 5% serum-
842 containing DMEM, respectively. The viral input was left for the duration of the experiment and
843 cells lysed at 48 h post-infection for RT-qPCR analysis.
844
845 **Statistical analyses.** Statistical analyses were performed with GraphPad Prism. Analysis types
846 are mentioned in Fig. legends and all comparisons are relative to the indicated controls. For
847 data with experimental factors greater than two, multiple linear regression was performed. For
848 data with two categorical factors, ANOVA was used, and repeated measures ANOVA when a
849 pairing factor was present. Simple linear regression was used when the relationship between a
850 continuous factor and a continuous response variable was investigated. P values are denoted
851 as follow: ns not significant, $p<0.05$ *, $p<0.01$ **, $p<0.001$ ***, $p<0.0001$****.
852
853
854 **Data availability**
855 The datasets generated during and/or analysed during the current study are available from the
856 corresponding author on reasonable request.
857
858

859 **Requests for materials**

860 Requests for material should be addressed to Caroline Goujon at the corresponding address
861 above.

862

863

864 **Acknowledgements**

865 We wish to thank Tom Doyle and Chad Swanson for their useful comments on the manuscript,
866 and Matthieu Lewis, Nadine Laguette, Nathalie Arhel, Juliette Fernandez, Jean-Luc Battini,
867 Georg Kochs, Andres Merits, Frédéric Tangy, Sylvie van de Werf and Nathan Sherer for the
868 generous provision of reagents, protocols and/or for helpful discussions. We are grateful to
869 Nicolas Manel and Helena Izquierdo-Fernandez for sharing their protocol for efficient
870 knockdown in primary CD4+ T cell using CRISPR/Cas9 RNP electroporation. We are grateful to
871 Myriam Boyer, Stéphanie Viala, Baptiste Monterroso and Orestis Faklaris from the imaging and
872 flow cytometry facility MRI, for advice with flow cytometry and confocal microscopy,
873 respectively. This work was supported by the Institut National de la Santé et de la Recherche
874 Médicale (INSERM) (to CG), the ATIP-Avenir programme (to CG), institutional funds from the
875 Centre National de la Recherche Scientifique (CNRS) and Montpellier University, France
876 REcherche Nord&Sud Sida/HIV et Hépatites (ANRS) (ECTZ21792 to CG; ECTZ35478 to OM),
877 Sidaction (to CG), a Starting Grant from the European Research Council (759226, ANTIViR) (to
878 CG), PhD studentships from the Ministry of Higher Education and Research (to BB, JM and
879 AR), and a 4th year PhD studentship from the Fondation pour la Recherche Médicale (to BB,
880 FDT201904008024). SR and HP acknowledge financial support from the France Génomique
881 National infrastructure, funded as part of "Investissement d'Avenir" program managed by
882 Agence Nationale de la Recherche (contract ANR-10-INBS-09). We acknowledge the imaging
883 facility MRI, member of the national infrastructure France-BioImaging supported by the French
884 National Research Agency (ANR-10-INBS-04) and the BSL-3 facility CEMIPAI (UAR 3725
885 CNRS Montpellier University).

886

887

888 **Author contributions**

889 B.B. and CG designed the study, analysed the data and wrote the manuscript. B.B. and C.G.
890 performed the whole-genome screens and candidate validation. B.B. carried out most of the
891 experiments, with technical assistance from A.R., F.G.d.G, J.M., M.T., W.D., A.M., A.L.C.V.,
892 M.A.A., and O.M.; V.C. provided some of the lentiviral vector stocks; E.B. and L.B. performed
893 CHIKV infections, N.G. performed ZIKV-Nluc infections, S.G. and N.J. performed MeV, ZIKV
894 PF13, DENV-2 and YFV infections; M.L and E.R analysed the RNA-seq data; R.S. performed
895 the statistical analyses; H.P. and S.R. performed the Illumina sequencing and MaGECK
896 analyses, respectively. All authors have read and approved the manuscript.

897 **Conflicts of interest statement**

898 The authors have no conflicts of interest to declare in relation to this manuscript.

References

1. Schoggins,J.W. (2019) Interferon-Stimulated Genes: What Do They All Do? *Annu. Rev. Virol.*, 6, 567–584.

2. Lindenmann,J. (1962) Resistance of mouse to mice adapted influenza A virus. *Virology*, 16, 203–204.

3. Zhou,A. (1993) Expression cloning of 2-5A-dependent RNAase: A uniquely regulated mediator of interferon action. *Cell*, 72, 753–765.

4. Zilberstein,A., Kimchi,A., Schmidt,A. and Revel,M. (1978) Isolation of two interferon-induced translational inhibitors: a protein kinase and an oligo-isoadenylate synthetase. *Proc. Natl. Acad. Sci.*, 75, 4734–4738.

5. Kane,M., Zang,T.M., Rihn,S.J., Zhang,F., Kueck,T., Alim,M., Schoggins,J., Rice,C.M., Wilson,S.J. and Bieniasz,P.D. (2016) Identification of Interferon-Stimulated Genes with Antiretroviral Activity. *Cell Host Microbe*, 20, 392–405.

6. OhAinle,M., Helms,L., Vermeire,J., Roesch,F., Humes,D., Basom,R., Delrow,J.J., Overbaugh,J. and Emerman,M. (2018) A virus-packageable CRISPR screen identifies host factors mediating interferon inhibition of HIV. *eLife*, 7, e39823.

7. Schoggins,J.W., Wilson,S.J., Panis,M., Murphy,M.Y., Jones,C.T., Bieniasz,P. and Rice,C.M. (2011) A diverse range of gene products are effectors of the type I interferon antiviral response. *Nature*, 472, 481–485.

8. Chemudupati,M., Kenney,A.D., Bonifati,S., Zani,A., McMichael,T.M., Wu,L. and Yount,J.S. (2019) From APOBEC to ZAP: Diverse mechanisms used by cellular restriction factors to inhibit virus infections. *Biochim. Biophys. Acta Mol. Cell Res.*, 1866, 382–394.

9. Doyle,T., Goujon,C. and Malim,M.H. (2015) HIV-1 and interferons: who's interfering with whom? *Nat. Rev. Microbiol.*, 13, 403–413.

10. Ghimire,D., Rai,M. and Gaur,R. (2018) Novel host restriction factors implicated in HIV-1 replication. *J. Gen. Virol.*, 99, 435–446.

11. Goujon,C., Moncorgé,O., Bauby,H., Doyle,T., Ward,C.C., Schaller,T., Hué,S., Barclay,W.S., Schulz,R. and Malim,M.H. (2013) Human MX2 is an interferon-induced post-entry inhibitor of HIV-1 infection. *Nature*, 502, 559–562.

12. Kane,M., Yadav,S.S., Bitzegeio,J., Kutluay,S.B., Zang,T., Wilson,S.J., Schoggins,J.W., Rice,C.M., Yamashita,M., Hatziioannou,T., *et al.* (2013) MX2 is an interferon-induced inhibitor of HIV-1 infection. *Nature*, 502, 563–566.

13. Jimenez-Guardeño,J.M., Apolonia,L., Betancor,G. and Malim,M.H. (2019) Immunoproteasome activation enables human TRIM5α restriction of HIV-1. *Nat. Microbiol.*, 10.1038/s41564-019-0402-0.

14. Fan,W., Mar,K.B., Sari,L., Gaszek,I.K., Cheng,Q., Evers,B.M., Shelton,J.M., Wight-Carter,M., Siegwart,D.J., Lin,M.M., *et al.* (2021) TRIM7 inhibits enterovirus replication and promotes emergence of a viral variant with increased pathogenicity. *Cell*, 184, 3410-3425.e17.

938 15. Shalem,O., Sanjana,N.E., Hartenian,E., Shi,X., Scott,D.A., Mikkelsen,T.S., Heckl,D.,
939 Ebert,B.L., Root,D.E., Doench,J.G., *et al.* (2014) Genome-scale CRISPR-Cas9 knockout
940 screening in human cells. *Science*, 343, 84–87.

941 16. Shalem,O., Sanjana,N.E. and Zhang,F. (2015) High-throughput functional genomics using
942 CRISPR-Cas9. *Nat. Rev. Genet.*, 16, 299–311.

943 17. Sanjana,N.E., Shalem,O. and Zhang,F. (2014) Improved vectors and genome-wide libraries
944 for CRISPR screening. *Nat. Methods*, 11, 783–784.

945 18. Li,W., Xu,H., Xiao,T., Cong,L., Love,M.I., Zhang,F., Irizarry,R.A., Liu,J.S., Brown,M. and
946 Liu,X.S. (2014) MAGeCK enables robust identification of essential genes from genome-
947 scale CRISPR/Cas9 knockout screens. *Genome Biol.*, 15, 554.

948 19. Doench,J.G. (2018) Am I ready for CRISPR? A user's guide to genetic screens. *Nat. Rev.*
949 *Genet.*, 19, 67–80.

950 20. Goujon,C., Schaller,T., Galão,R.P., Amie,S.M., Kim,B., Olivieri,K., Neil,S.J.D. and
951 Malim,M.H. (2013) Evidence for IFNα-induced, SAMHD1-independent inhibitors of early
952 HIV-1 infection. *Retrovirology*, 10, 23.

953 21. Bulli,L., Apolonia,L., Kutzner,J., Pollpeter,D., Goujon,C., Herold,N., Schwarz,S.-M.,
954 Giernat,Y., Keppler,O.T., Malim,M.H., *et al.* (2016) Complex interplay between HIV-1
955 Capsid and MX2-independent IFNα-induced antiviral factors. *J. Virol.*,
956 10.1128/JVI.00458-16.

957 22. Xu,B., Pan,Q. and Liang,C. (2018) Role of MxB in Alpha Interferon-Mediated Inhibition of
958 HIV-1 Infection. *J. Virol.*, 92.

959 23. Uhlmann-Schiffler,H., Jalal,C. and Stahl,H. (2006) Ddx42p--a human DEAD box protein with
960 RNA chaperone activities. *Nucleic Acids Res.*, 34, 10–22.

961 24. Taschuk,F. and Cherry,S. (2020) DEAD-Box Helicases: Sensors, Regulators, and Effectors
962 for Antiviral Defense. *Viruses*, 12.

963 25. Granneman,S., Bernstein,K.A., Bleichert,F. and Baserga,S.J. (2006) Comprehensive
964 Mutational Analysis of Yeast DEXD/H Box RNA Helicases Required for Small Ribosomal
965 Subunit Synthesis. *Mol. Cell. Biol.*, 26, 1183–1194.

966 26. Rocak,S. (2005) Characterization of the ATPase and unwinding activities of the yeast
967 DEAD-box protein Has1p and the analysis of the roles of the conserved motifs. *Nucleic*
968 *Acids Res.*, 33, 999–1009.

969 27. Ochsenbauer,C., Edmonds,T.G., Ding,H., Keele,B.F., Decker,J., Salazar,M.G., Salazar-
970 Gonzalez,J.F., Shattock,R., Haynes,B.F., Shaw,G.M., *et al.* (2012) Generation of
971 transmitted/founder HIV-1 infectious molecular clones and characterization of their
972 replication capacity in CD4 T lymphocytes and monocyte-derived macrophages. *J. Virol.*,
973 86, 2715–2728.

974 28. Uhlmann-Schiffler,H., Kiermayer,S. and Stahl,H. (2009) The DEAD box protein Ddx42p
975 modulates the function of ASPP2, a stimulator of apoptosis. *Oncogene*, 28, 2065–2073.

976 29. Zyner,K.G., Mulhearn,D.S., Adhikari,S., Martínez Cuesta,S., Di Antonio,M., Erard,N.,
977 Hannon,G.J., Tannahill,D. and Balasubramanian,S. (2019) Genetic interactions of G-
978 quadruplexes in humans. *eLife*, 8.

979 30. Faulkner,G.J. and Billon,V. (2018) L1 retrotransposition in the soma: a field jumping ahead.
980 *Mob. DNA*, 9, 22.

981 31. Liu,N., Lee,C.H., Swigut,T., Grow,E., Gu,B., Bassik,M.C. and Wysocka,J. (2018) Selective
982 silencing of euchromatic L1s revealed by genome-wide screens for L1 regulators.
983 *Nature*, 553, 228–232.

984 32. Moran,J.V., Holmes,S.E., Naas,T.P., DeBerardinis,R.J., Boeke,J.D. and Kazazian,H.H.
985 (1996) High frequency retrotransposition in cultured mammalian cells. *Cell*, 87, 917–927.

986 33. Wei,J., Alfajaro,M.M., DeWeirdt,P.C., Hanna,R.E., Lu-Culligan,W.J., Cai,W.L., Strine,M.S.,
987 Zhang,S.-M., Graziano,V.R., Schmitz,C.O., *et al.* (2020) Genome-wide CRISPR screens
988 reveal host factors critical for SARS-CoV-2 infection. *Cell*, 10.1016/j.cell.2020.10.028.

989 34. Haller,O., Staeheli,P., Schwemmle,M. and Kochs,G. (2015) Mx GTPases: dynamin-like
990 antiviral machines of innate immunity. *Trends Microbiol.*, 23, 154–163.

991 35. Burdick,R.C., Li,C., Munshi,M., Rawson,J.M.O., Nagashima,K., Hu,W.-S. and Pathak,V.K.
992 (2020) HIV-1 uncoats in the nucleus near sites of integration. *Proc. Natl. Acad. Sci.*, 117,
993 5486–5493.

994 36. Dharan,A., Bachmann,N., Talley,S., Zwikelmaier,V. and Campbell,E.M. (2020) Nuclear pore
995 blockade reveals that HIV-1 completes reverse transcription and uncoating in the
996 nucleus. *Nat. Microbiol.*, 10.1038/s41564-020-0735-8.

997 37. Peng,K., Muranyi,W., Glass,B., Laketa,V., Yant,S.R., Tsai,L., Cihlar,T., Müller,B. and
998 Kräusslich,H.-G. (2014) Quantitative microscopy of functional HIV post-entry complexes
999 reveals association of replication with the viral capsid. *eLife*, 3, e04114.

1000 38. Zyner,K.G., Mulhearn,D.S., Adhikari,S., Martínez Cuesta,S., Di Antonio,M., Erard,N.,
1001 Hannon,G.J., Tannahill,D. and Balasubramanian,S. (2019) Genetic interactions of G-
1002 quadruplexes in humans. *eLife*, 8, e46793.

1003 39. Fay,M.M., Lyons,S.M. and Ivanov,P. (2017) RNA G-Quadruplexes in Biology: Principles and
1004 Molecular Mechanisms. *J. Mol. Biol.*, 429, 2127–2147.

1005 40. Ruggiero,E. and Richter,S.N. (2018) G-quadruplexes and G-quadruplex ligands: targets and
1006 tools in antiviral therapy. *Nucleic Acids Res.*, 46, 3270–3283.

1007 41. Will,C.L., Urlaub,H., Achsel,T., Gentzel,M., Wilm,M. and Lührmann,R. (2002)
1008 Characterization of novel SF3b and 17S U2 snRNP proteins, including a human Prp5p
1009 homologue and an SF3b DEAD-box protein. *EMBO J.*, 21, 4978–4988.

1010 42. Will,C.L., Urlaub,H., Achsel,T., Gentzel,M., Wilm,M. and Lührmann,R. (2002)
1011 Characterization of novel SF3b and 17S U2 snRNP proteins, including a human Prp5p
1012 homologue and an SF3b DEAD-box protein. *EMBO J.*, 21, 4978–4988.

1013 43. Moy,R.H., Cole,B.S., Yasunaga,A., Gold,B., Shankarling,G., Varble,A., Molleston,J.M.,
1014 tenOever,B.R., Lynch,K.W. and Cherry,S. (2014) Stem-loop recognition by DDX17
1015 facilitates miRNA processing and antiviral defense. *Cell*, 158, 764–777.

1016 44. Xu,Y.-Z., Newnham,C.M., Kameoka,S., Huang,T., Konarska,M.M. and Query,C.C. (2004)
1017 Prp5 bridges U1 and U2 snRNPs and enables stable U2 snRNP association with intron
1018 RNA. *EMBO J.*, 23, 376–385.

1019 45. Zheng,Q., Hou,J., Zhou,Y., Li,Z. and Cao,X. (2017) The RNA helicase DDX46 inhibits innate
1020 immunity by entrapping m6A-demethylated antiviral transcripts in the nucleus. *Nat.*
1021 *Immunol.*, 18, 1094–1103.

1022 46. Goujon,C., Arfi,V., Pertel,T., Luban,J., Lienard,J., Rigal,D., Darlix,J.-L. and Cimarelli,A.
1023 (2008) Characterization of Simian Immunodeficiency Virus SIVSM/Human
1024 Immunodeficiency Virus Type 2 Vpx Function in Human Myeloid Cells. *J. Virol.*, 82,
1025 12335–12345.

1026 47. Doyle,T., Moncorgé,O., Bonaventure,B., Pollpeter,D., Lussignol,M., Tauziet,M., Apolonia,L.,
1027 Catanese,M.-T., Goujon,C. and Malim,M.H. (2018) The interferon-inducible isoform of
1028 NCOA7 inhibits endosome-mediated viral entry. *Nat. Microbiol.*, 3, 1369–1376.

1029 48. Rebendenne,A., Valadão,A.L.C., Tauziet,M., Maarifi,G., Bonaventure,B., McKellar,J.,
1030 Planès,R., Nisole,S., Arnaud-Arnould,M., Moncorgé,O., *et al.* (2021) SARS-CoV-2
1031 triggers an MDA-5-dependent interferon response which is unable to control replication
1032 in lung epithelial cells. *J. Virol.*, 10.1128/JVI.02415-20.

1033 49. Moncorge,O., Long,J.S., Cauldwell,A.V., Zhou,H., Lycett,S.J. and Barclay,W.S. (2013)
1034 Investigation of Influenza Virus Polymerase Activity in Pig Cells. *J. Virol.*, 87, 384–394.

1035 50. Adachi,A., Gendelman,H.E., Koenig,S., Folks,T., Willey,R., Rabson,A. and Martin,M.A.
1036 (1986) Production of acquired immunodeficiency syndrome-associated retrovirus in
1037 human and nonhuman cells transfected with an infectious molecular clone. *J. Virol.*, 59,
1038 284–291.

1039 51. Simon,J.H., Southerling,T.E., Peterson,J.C., Meyer,B.E. and Malim,M.H. (1995)
1040 Complementation of vif-defective human immunodeficiency virus type 1 by primate, but
1041 not nonprimate, lentivirus vif genes. *J. Virol.*, 69, 4166–4172.

1042 52. Schaller,T., Ocwieja,K.E., Rasaiyaah,J., Price,A.J., Brady,T.L., Roth,S.L., Hué,S.,
1043 Fletcher,A.J., Lee,K., KewalRamani,V.N., *et al.* (2011) HIV-1 capsid-cyclophilin
1044 interactions determine nuclear import pathway, integration targeting and replication
1045 efficiency. *PLoS Pathog.*, 7, e1002439.

1046 53. Ryan-Graham,M.A. and Peden,K.W.C. (1995) Both Virus and Host Components Are
1047 Important for the Manifestation of a Nef- Phenotype in HIV-1 and HIV-2. *Virology*, 213,
1048 158–168.

1049 54. Gaddis,N.C., Sheehy,A.M., Ahmad,K.M., Swanson,C.M., Bishop,K.N., Beer,B.E., Marx,P.A.,
1050 Gao,F., Bibollet-Ruche,F., Hahn,B.H., *et al.* (2004) Further Investigation of Simian
1051 Immunodeficiency Virus Vif Function in Human Cells. *J. Virol.*, 78, 12041–12046.

1052 55. Naldini,L., Blömer,U., Gallay,P., Ory,D., Mulligan,R., Gage,F.H., Verma,I.M. and Trono,D.
1053 (1996) In vivo gene delivery and stable transduction of nondividing cells by a lentiviral
1054 vector. *Science*, 272, 263–267.

1055 56. Bainbridge,J.W., Stephens,C., Parsley,K., Demaison,C., Halfyard,A., Thrasher,A.J. and
1056 Ali,R.R. (2001) In vivo gene transfer to the mouse eye using an HIV-based lentiviral
1057 vector; efficient long-term transduction of corneal endothelium and retinal pigment
1058 epithelium. *Gene Ther.*, 8, 1665–1668.

1059 57. O'Rourke,J.P., Newbound,G.C., Kohn,D.B., Olsen,J.C. and Bunnell,B.A. (2002) Comparison
1060 of gene transfer efficiencies and gene expression levels achieved with equine infectious

1061 anemia virus- and human immunodeficiency virus type 1-derived lentivirus vectors. *J.*
1062 *Virol.*, 76, 1510–1515.

1063 58. Saenz,D.T., Teo,W., Olsen,J.C. and Poeschla,E.M. (2005) Restriction of feline
1064 immunodeficiency virus by Ref1, Lv1, and primate TRIM5alpha proteins. *J. Virol.*, 79,
1065 15175–15188.

1066 59. Ostertag,E.M., Prak,E.T., DeBerardinis,R.J., Moran,J.V. and Kazazian,H.H. (2000)
1067 Determination of L1 retrotransposition kinetics in cultured cells. *Nucleic Acids Res.*, 28,
1068 1418–1423.

1069 60. Goodier,J.L., Cheung,L.E. and Kazazian,H.H. (2012) MOV10 RNA Helicase Is a Potent
1070 Inhibitor of Retrotransposition in Cells. *PLoS Genet.*, 8, e1002941.

1071 61. Zhong,J., Gastaminza,P., Cheng,G., Kapadia,S., Kato,T., Burton,D.R., Wieland,S.F.,
1072 Uprichard,S.L., Wakita,T. and Chisari,F.V. (2005) Robust hepatitis C virus infection in
1073 vitro. *Proc. Natl. Acad. Sci. U. S. A.*, 102, 9294–9299.

1074 62. Nakabayashi,H., Taketa,K., Miyano,K., Yamane,T. and Sato,J. (1982) Growth of human
1075 hepatoma cells lines with differentiated functions in chemically defined medium. *Cancer*
1076 *Res.*, 42, 3858–3863.

1077 63. Wingett,S.W. and Andrews,S. (2018) FastQ Screen: A tool for multi-genome mapping and
1078 quality control. *F1000Research*, 7, 1338.

1079 64. Martin,M. (2011) Cutadapt removes adapter sequences from high-throughput sequencing
1080 reads. *EMBnet.journal*, 17, 10–12.

1081 65. Langmead,B., Trapnell,C., Pop,M. and Salzberg,S.L. (2009) Ultrafast and memory-efficient
1082 alignment of short DNA sequences to the human genome. *Genome Biol.*, 10, R25.

1083 66. Li,H., Handsaker,B., Wysoker,A., Fennell,T., Ruan,J., Homer,N., Marth,G., Abecasis,G.,
1084 Durbin,R., and 1000 Genome Project Data Processing Subgroup (2009) The Sequence
1085 Alignment/Map format and SAMtools. *Bioinforma. Oxf. Engl.*, 25, 2078–2079.

1086 67. Goujon,C. and Malim,M.H. (2010) Characterization of the alpha interferon-induced postentry
1087 block to HIV-1 infection in primary human macrophages and T cells. *J. Virol.*, 84, 9254–
1088 9266.

1089 68. Corman,V.M., Landt,O., Kaiser,M., Molenkamp,R., Meijer,A., Chu,D.K., Bleicker,T.,
1090 Brünink,S., Schneider,J., Schmidt,M.L., *et al.* (2020) Detection of 2019 novel coronavirus
1091 (2019-nCoV) by real-time RT-PCR. *Euro Surveill. Bull. Eur. Sur Mal. Transm. Eur.*
1092 *Commun. Dis. Bull.*, 25.

1093 69. Meertens,L., Hafirassou,M.L., Couderc,T., Bonnet-Madin,L., Kril,V., Kümmerer,B.M.,
1094 Labeau,A., Brugier,A., Simon-Loriere,E., Burlaud-Gaillard,J., *et al.* (2019) FHL1 is a
1095 major host factor for chikungunya virus infection. *Nature*, 574, 259–263.

1096 70. Zürcher,T., de la Luna,S., Sanz-Ezquerro,J.J., Nieto,A. and Ortín,J. (1996) Mutational
1097 analysis of the influenza virus A/Victoria/3/75 PA protein: studies of interaction with PB1
1098 protein and identification of a dominant negative mutant. *J. Gen. Virol.*, 77 (Pt 8), 1745–
1099 1749.

1100 71. Schindelin,J., Arganda-Carreras,I., Frise,E., Kaynig,V., Longair,M., Pietzsch,T., Preibisch,S.,
1101 Rueden,C., Saalfeld,S., Schmid,B., *et al.* (2012) Fiji: an open-source platform for
1102 biological-image analysis. *Nat. Methods*, 9, 676–682.

1103 72. Rentsch,M.B. and Zimmer,G. (2011) A Vesicular Stomatitis Virus Replicon-Based Bioassay
1104 for the Rapid and Sensitive Determination of Multi-Species Type I Interferon. *PLoS ONE*,
1105 6.

1106 73. Combredet,C., Labrousse,V., Mollet,L., Lorin,C., Delebecque,F., Hurtrel,B., McClure,H.,
1107 Feinberg,M.B., Brahic,M. and Tangy,F. (2003) A molecularly cloned Schwarz strain of
1108 measles virus vaccine induces strong immune responses in macaques and transgenic
1109 mice. *J. Virol.*, 77, 11546–11554.

1110 74. Mutso,M., Saul,S., Rausalu,K., Susova,O., Žusinaite,E., Mahalingam,S. and Merits,A.
1111 (2017) Reverse genetic system, genetically stable reporter viruses and packaged
1112 subgenomic replicon based on a Brazilian Zika virus isolate. *J. Gen. Virol.*, 98, 2712–
1113 2724.

1114